Optimization of Capacitive Micromachined Ultrasound Transducers (CMUTs) for a High-Frequency Medical Ultrasonic Imaging System

by

Reza Pakdaman Zangabad

Submitted to the Graduate School of Engineering and Natural Sciences

in partial fulfillment of

the requirements for the degree of

Master of Science

Sabancı University

Summer, 2014

Optimization of Capacitive Micromachined Ultrasound Transducers (CMUTs) for High-Frequency Medical Ultrasonic Imaging System

APPROVED BY

Assoc. Prof. Dr. Ayhan BOZKURT

....

(Thesis Supervisor)

Prof. Dr. İbrahim TEKİN

....

Assoc. Prof. Dr. Arif Sanlı Ergün (TOBB
ETU)

....

DATE OF APPROVAL: ....

iii

Optimization of Capacitive Micromachined Ultrasound Transducers (CMUTs) for High-Frequency Medical Ultrasonic Imaging System

Keywords: High Frequency CMUT, High Resolution Medical Imaging, Pulse-Echo Optimization, Circuit Model for Ultrasonic Imaging.

Abstract

Conventional ultrasonic imaging systems use piezoelectric transducers for the generation and reception of the acoustic signal. Since its invention in 1994, the Capacitive Micromachined Ultrasound Transducer (CMUT) has been subjected to research as an alternative technology. Major advantages of the CMUT over traditional piezoelectric ultrasound transducers include higher bandwidth, higher sensitivity, CMOS compatibility, and ease of manufacturing (by the use of standard lithography techniques.) Increasing the dynamic range, decreasing the parasitic capacitance and cross coupling are the major goals in CMUT designing specially for medical imaging applications. The work in this thesis aims the optimization of a high-frequency (20 MHz) CMUT array to be used for high-resolution medical imaging. The figure of merit has been chosen as the signal-to-noise ratio of the electrical return signal, which required the construction of a model for the entire pulse-echo operation. Such a model consists of: (1) a circuit model for the device itself, (2) a model for the radiation impedance, and (3) a model for the propagation medium. The CMUT model has been extensively studied in the literature. An already existing circuit model has been used in the simulations. The radiation impedance of the CMUT array was computed using Finite Element Analysis (FEA) software packages COMSOL Multiphysics® and ANSYS®, and converted to an equivalent circuit to represent the load in the circuit simulator. The pulse-echo model, which is entirely implemented in LTspice circuit simulator, was then used to optimize CMUT parameters that include radius, membrane thickness, and gap height to maximize signal-to-noise ratio.

Yüksek Frekans Tıbbi Ultrasonik Görüntüleme Sistemleri İçin Kapasitif Mikroişlenmiş Ultrasonik Dönüştürücülerin (CMUTs) Optimizasyonu

Anahtar Kelimeler: Yüksek Frekanslı CMUT, Yüksek Çözünürlüklü Tıbbi Görüntüleme, Darbe-eko Optimizasiyonu, Ultrasonik Görüntüleme İçin Devre Modeli

Özet

Geleneksel ultrasonik görüntüleme sistemleri, akustik sinyalin üretimi ve alımı için piezoelektrik dönüştürücüler kullanmaktadırlar. 1994 yılında bulunmasından bu yana, Kapasitif Mikroişlenmiş Ultrason Dönüştürücü (CMUT) alternatif bir teknoloji olarak araştırmaya tabi olmuştur. Geleneksel piezoelektrik ultrason dönüştürücüler üzerinde CMUT'ın önemli avantajları daha yüksek bant genişliği, daha yüksek hassasiyet, CMOS uyumluluk ve standart litografi teknikleri kullanılmasıyla elde edilen imalat kolaylığıdır. Özellikle tıbbi görüntüleme uygulamaları için geliştirilen CMUT tasarımlarında parazitik kapasiteleri ve eşleşmeleri azaltmak, dinamik aralığı artırmak önemli amaçlardır. Bu tezde yüksek çözünürlüklü medikal görüntüleme için kullanılacak yüksek frekanslı (20 MHz) CMUT dizisinin optimizasyonu amaçlamaktadır. Başari ölçütü, bütün darbe-eko işlemi için bir modelin geliştirilmesi için gereken elektrik geri dönüş sinyalinin sinyal-gürültü oranı olarak seçilmiştir. Bu tür bir model aşağıdakilerden oluşmaktadır (1) cihazın kendisi için bir devre modeli, (2), radyasyon empedansı için bir model ve (3) Yayılma ortamı için model.

CMUT model literatürde çok araştırılmıştır. Zaten varolan bir devre modeli simülasyonlarda kullanılmıştır.CMUT dizi yayın empedansı, Sonlu Eleman Analizi (FEA) yazılım paketleri ile COMSOL Multiphysics ve ANSYS kullanılarak hesaplanmıştır, ve devre simülatöründeki yükü temsil etmek üzere bir eşdeğer devre modele dönüştürülmüştür. Tümüyle LT SPİCE devre simülatöründe gerçeklenen darbe-eko modeliyle CMUT parametrelerinden yarıçap, membran kalınlığı ve boşluk boyu kullanilarak sinyal gürültü orani optimize edilmiştir.

Contents

List of Figures

ix

x

List of Tables

1. Introduction

Capacitive Micromachined Ultrasound Transducer (CMUT) [1-3] is a flexible membrane suspended over a substrate with spacing in sub-micrometer range. Two electrodes are placed in membrane and substrate in parallel-plate capacitor configuration, actuating the device in ultrasound frequencies. Ultrasound is a type of acoustic wave with frequencies above the audible range of human beings (>20 kHz). CMUT applications mostly include air-coupled nondestructive testing [4-5], medical imaging [6-8], and High Intensity Focused Ultrasound (HIFU) [9-10]. There are many advantages and challenges regarding the CMUT arrays in comparison with traditional piezoelectric transducers. Advantages of CMUT array are mentioned such as improved impedance match in both fluid and air [15-16].With good impedance matching it is possible to reach wider bandwidths. Piezoelectric transducers have fractional bandwidths of 60%-80%, however fractional bandwidth above the 100% can be easily achieved using CMUTs. The bandwidth is an important parameter in determining the image resolution: wider bandwidths result in better image resolution. In-vitro comparison of image quality between CMUT arrays and piezoelectric transducers

shows improvement in the radial resolution [17-18], significant enhance in the contrast, and field of view in images received from CMUT arrays [19].

Another great advantage of CMUT over piezoelectric transducers is the manufacturing process. The photolithographic techniques enable very small dimensions both in depth and laterally and meet the needs for small elements and minimal distance between adjacent elements which is important factor in high frequency ultrasound imaging. Micromachining fabrication involves parallel processing of several wafers; hence, the production cost can be low when a process is optimized. Also the integration of CMUT and transmit circuitry can be realized using through wafer vias and 3D-stacking of the transducer chip and several IC chips [20-21].

Drawback of CMUT in medical imaging is low sensitivity leading to limited penetration depth [22-23]. Different membrane sizes and shapes have been proposed to increase the transmission and reception efficiency such as using rectangular configuration [24]. Also dual electrode CMUT configuration is proposed to enhance the receive mode sensitivity [25-26].

Charging effect is another problem in CMUT and MEMS devices [27-30]. Due to the strong electric field within the transducer cavity or during the fabrication process, the charging effect may happen. This phenomenon may prevent the membrane from snapping-back after collapse in collapse mode operation regime of CMUT due to the creation of electrostatic force results in degraded performance and reliability and lifetime of device [31].

One of most important phenomena which affects device performance and should be controlled is acoustic cross-talk. It happens between fluid-structure interfaces and also through the supporting structure (substrate). Creation of acoustic waves due to the vibration of CMUT membrane is coupled to adjacent element and degrades the CMUT array performance. Surface Acoustic Waves (SAWs) propagate through substrate and dispersive guided modes which are generated in fluid-CMUT interfaces are two main contributions of acoustic cross-talk in CMUT arrays [32-33]. CMUT membrane vibration creates longitudinal waves propagating into the substrate which maybe reflected from bottom of substrate and picked up by CMUT and consequently degrade

2

the radiation pattern of array. Using the backing layer in substrate is proposed as a solution [34-35].Thinning the substrate to increase the substrate resonance frequency to levels above the frequency range of interest is another solution. However, in thin silicon substrates, plate modes, such as Lamb waves may be excited [36]. One solution to overcome this problem is introducing deep trench isolation between neighboring CMUT elements [37].

1.1 CONTRIBUTION

Tunable parameters of the CMUT include the membrane material, radius and thickness, gap height, electrode size. The operation frequency, bandwidth, input and output sensitivity requirements may vary for different applications. Usually, improving one operational parameter results in the degradation of the other, hence a compromise solution is required. In medical imaging, for example, the device will be used in pulse-echo mode for which both good receive sensitivity and high output pressure is required. In this study, we investigate the round-trip behavior of the transducer and show that there is an optimal set of operational parameters that results in the largest pulse-echo signal output and best signal-to-noise ratio (SNR).

An optimization study can be conducted by the use of analytical and/or numerical models for the device. Circuit modeling of CMUT arrays is preferred upon the Finite Element Analysis (FEA) due to the time consumption of FEA and acceptable accuracy of circuit simulator. Recently, analytical and computational models for the CMUTs have been developed [11-14]. Nonlinear modeling of CMUT array demonstrated accurate results in comparison with FEA [38]. One important circuit component in lumped modeling of CMUT cell is the radiation impedance. Since fluid coupling through the immersion medium results in acoustic cross-talk, the radiation impedance model for a multitude of CMUT cells depends on the topology of CMUT elements and cell to cell spacing [39]. Existing models for the self and mutual radiation impedance of CMUT cells have been exploited for the construction of an equivalent circuit model with appropriate bandwidth, which is meticulously discussed in chapter 3.

The organization of this thesis is as follows:

Chapter 2 discusses high frequency medical ultrasound imaging systems and then deals with different operating regimes of the CMUT and shows possible plate modes of CMUT membrane.

Chapter 3 studies the three modeling types of an array of immersed circular CMUT: (i) analytically, (ii) finite Element Method (FEM), and (iii) equivalent circuit modeling.

Chapter 4 presents the design of circular CMUT array operating in 20 MHz and studies the optimizing the device parameters in order to achieve the largest return echo and the best signal-to-noise ratio for pulse-echo medical imaging system.

2. Medical Ultrasound Imaging

2.1 History

After Titanic Crashed into an iceberg and sank in 1912, Paul Langevin was commissioned to invent a device that detects the objects at the bottom of the sea. His inspiration by the Titanic sinking leaded to invent a first hydrophone in 1915, what the World Congress Ultrasound in Medical Education refers to as the first transducer. The development of first SOund Navigation And Ranging (SONAR) system where the distance to object were measured using transmission and reception of sound waves is accomplished during the World War I [40].

The knowledge of pulse-echo from SONAR and RADAR systems were eventuated in using the ultrasound technique in medicine after World War II when Karl Dussik, a neurologist and physicist at University of Vienna, used the ultrasound for medical diagnosis of human brain tumor in 1942. In 1948 George Ludwig first described the use of ultrasound in diagnosis of gallstones. Ultrasound scanners have become a popular diagnostic tool in many areas of medicine. Most well-known are probably abdominal and obstetric imaging and echocardiography (imaging of the heart).

5

Ultrasound is in most cases a non-invasive imaging technique. As long as guidelines are followed, it has no known harmful effects, which is an advantage compared to x-ray, computed tomography (CT) imaging and Positron Emission Tomography (PET). Another important advantage of ultrasound is its lower cost and that it is more portable than PET, CT scanners and magnetic resonance imaging (MRI). The portability of ultrasound scanners have improved dramatically during the last few years, when handheld and laptop size scanners have become available [41].

2.2 Working Principles of Ultrasound Imaging

In solids, sound waves can be both longitudinal and shear (transversal). In longitudinal waves, the particle motion is in the same direction as the wave, whereas in shear waves, the particles move perpendicular to the propagation direction of the wave. For a shear wave to travel, the medium must be rigid. As one particle begins to move it must be able to pull on its nearest neighbor. If the medium is not rigid as is the case with fluids, the particles will slide each other. This sliding action prevents one particle from pulling its neighbor in a direction perpendicular to the energy transport; hence, waves traveling through a bulk of fluid (liquid or gas) are always longitudinal. Human tissues are often modeled as a fluid due to high water content of human body. Hence, shear waves are usually disregarded in medical ultrasound modeling. However, the shear waves must be taken into account in transducer design, since the materials in the ultrasonic transducers are solids.
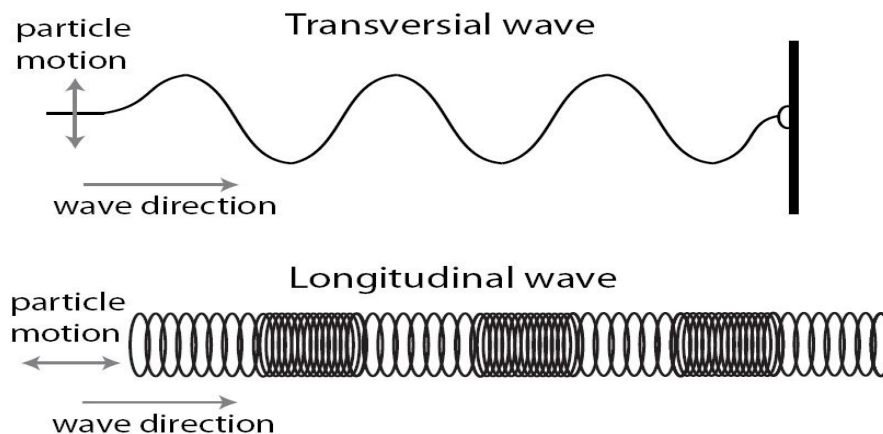
Figure 2-1: Shear and Longitudinal Wave illustration

6

The difference in acoustic impedance of various kinds of human tissue (e.g. fat, muscle, bone, connective tissue, blood) is the basis of ultrasonic imaging. To collect data for the image, an ultrasonic pulse is transmitted into the body by a transducer and as the wave hits the various layers of tissue, the wave will be partially transmitted and partially reflected as illustrated in Figure 2.2. The transducer then records the reflected signal and based on the time-of-flight, the system calculates the depth of the object which reflected the signal.

Material 0
$Z_0 = \rho_0 c_0$
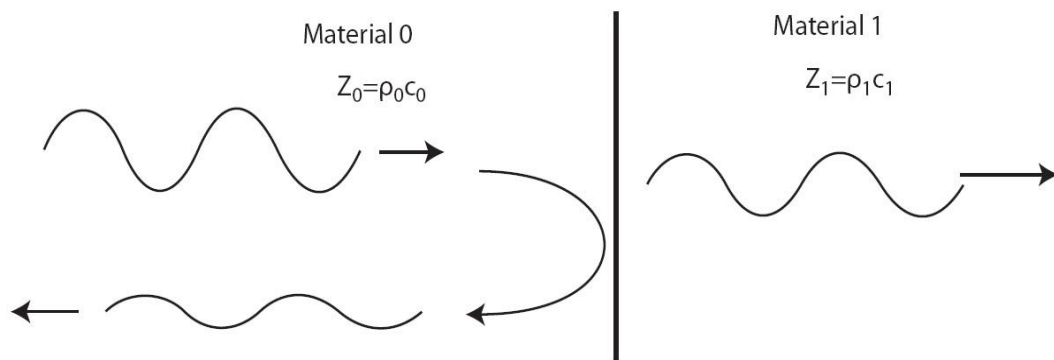
Material 1
$Z_1 = \rho_1 c_1$

Figure 2-2: Transmission and reflection of sound wave at the interface between two materials with different acoustic impedance

In order to construe an image, the beam steering of device should be used which is the sending ultrasound waves to many directions and recollecting the echo pulses from those directions. Beam steering can be done by two approaches: Mechanically beam steering and electronically beam scanning. As it is illustrated in Figure 2-3, mechanically beam steering involves the moving transducer with a motor in order to scan the desired area which has a lot of problems but at the other hand, electronically beam scanning is introducing the time delay for each element of transducer in array and is accurate at the cost of complexity of device.

7
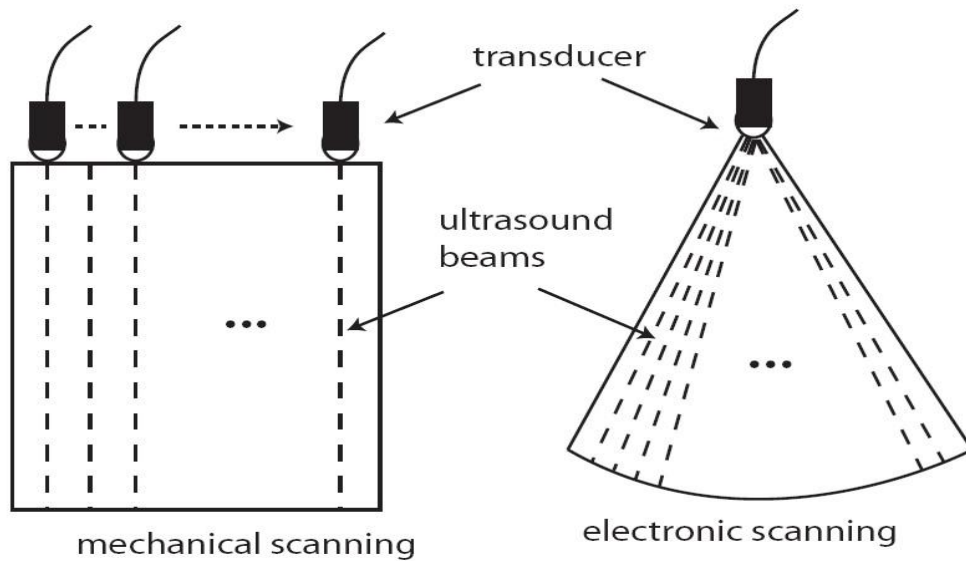
Figure 2-3: Beam steering and ultrasound image formation

2.3 Image Quality

In this section, the parameters that define the quality of the ultrasound image are considered. One of the most important parameter should be considered is the spatial resolution.

2.3.1 Spatial Resolution

Spatial resolution is the ability to distinguish between objects located at different positions in space. Spatial resolution is divided into two components: axial resolution and lateral resolution. Axial resolution is the ability to distinguish between echoes coming from two objects lying one behind the other along the axis of the ultrasound beam. It is sometimes refers as depth resolution. It is expresses as:

$$\Delta S = \frac{c \times T_p}{2} = \frac{c}{2 \times B}$$

Eq. 2-1

8

where *Tp* is the pulse length, *B* is the pulse bandwidth and *c* is the speed of sound inhuman tissue (~1540 m/s). Eq. 2.1 shows that the axial resolution is depended on operation frequency of transducer, pulse width and bandwidth of transducer.

Lateral resolution is the ability to distinguish between two objects placed side by side in a direction perpendicular to that of ultrasound beam. Figures 2-4 and 2-5 illustrate the axial and lateral resolution respectively. The lateral resolution depends on the beam width at the focus point which is defined as [42]:

$$\Delta l = k \frac{\lambda \times F}{D} = k.\lambda.f \,\#$$ Eq. 2-2

the $f\# = \frac{r}{a}$ where *r* is the focal depth and *a* is the active aperture of the transducer, *D* is the aperture size and *k* is a scaling constant. It is clear that the lateral resolution could be improved by increasing the frequency. The resolution will also be improved by small separation between the beams. The scaling constant depends on the shape of the transducer. The lateral resolution changes with depth while the radial resolution is quite constant with depth. Both the radial and lateral resolution will influence objects that are smaller than the resolution size. These objects will appear to be at least the resolution size even though the objects are smaller.
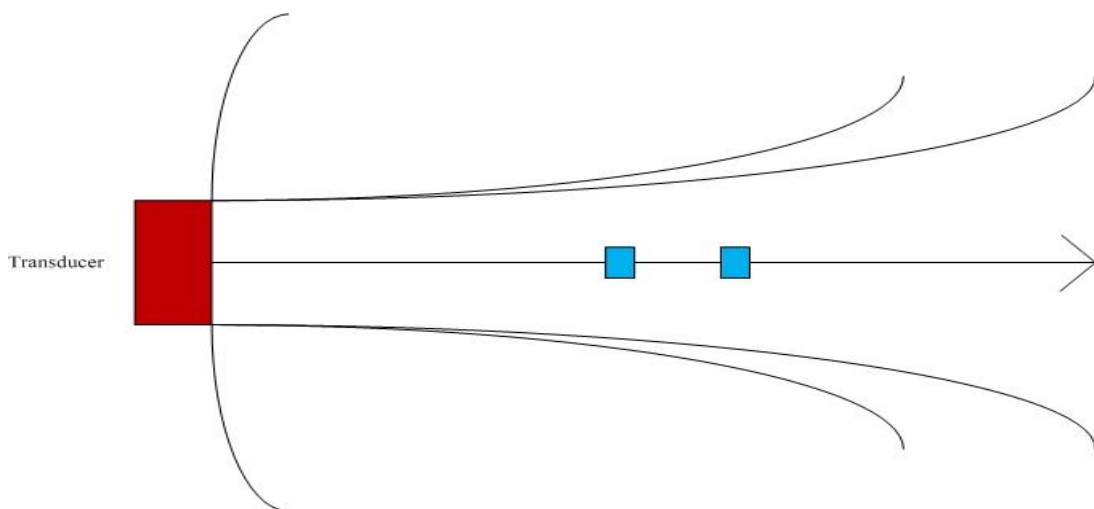
Figure 2-4: Axial resolution where objects are placed side by side along the beam direction

9
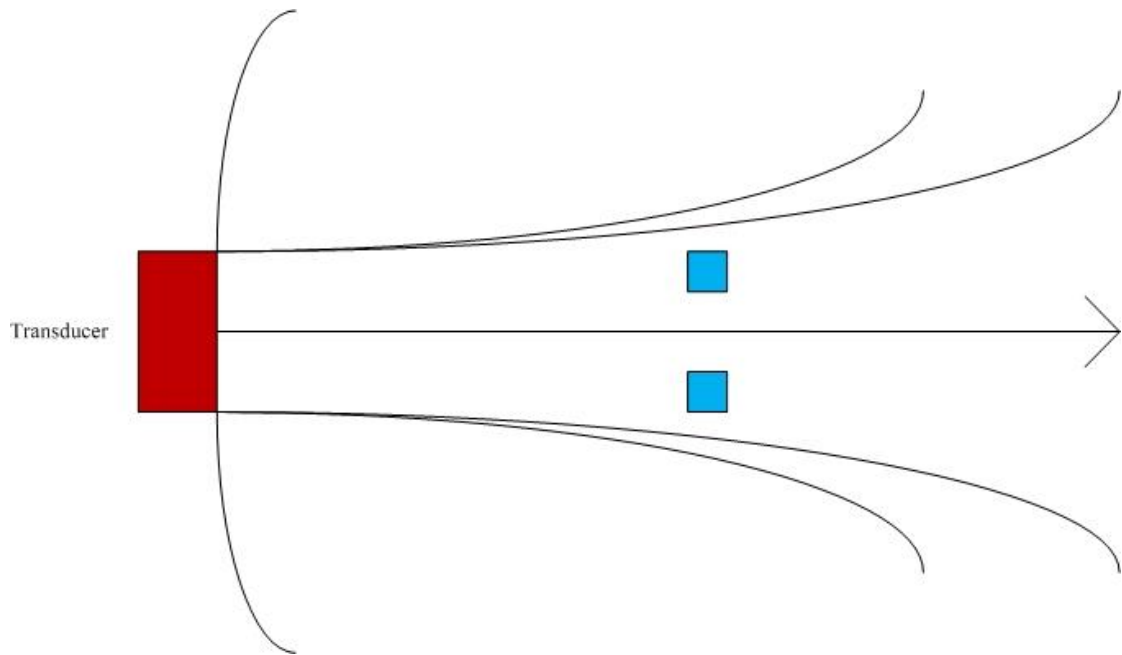
Figure 2-5: Lateral resolution where two objects are place side by side perpendicular to the beam direction

High frequency is good for the image resolution, however, as the operation frequency increases, the attenuation increases. For example the attenuation in human soft tissue is 0.5 dB/cm/MHz. Thus, high frequency transducers are best suited for superficial imaging applications.

3. Capacitive Micromachined Ultrasound Transducer

The Capacitive Micromachined Ultrasound transducer (CMUT) is a flexible membrane which first converts the electrical energy to mechanical energy as vibration and second converts the mechanical vibration to acoustic energy. CMUT has the potential of replacing the piezoelectric transducer especially in medical ultrasound field due to higher bandwidth and other prominent characteristics which have been discussed in the previous chapters. The following chapter will emphasize on CMUT operation principles and modeling techniques of CMUT array.

3.1 Basic Principles of CMUT

The basic operation principles of CMUT could be understood by examining the Figure 3-1 which depicts the cross section view of a single CMUT cell. As it can be inferred from the figure, a CMUT is a parallel plate structure constructing a capacitor. When a DC voltage is applied to embedded electrode in the membrane and grounded by substrate (bottom electrode),
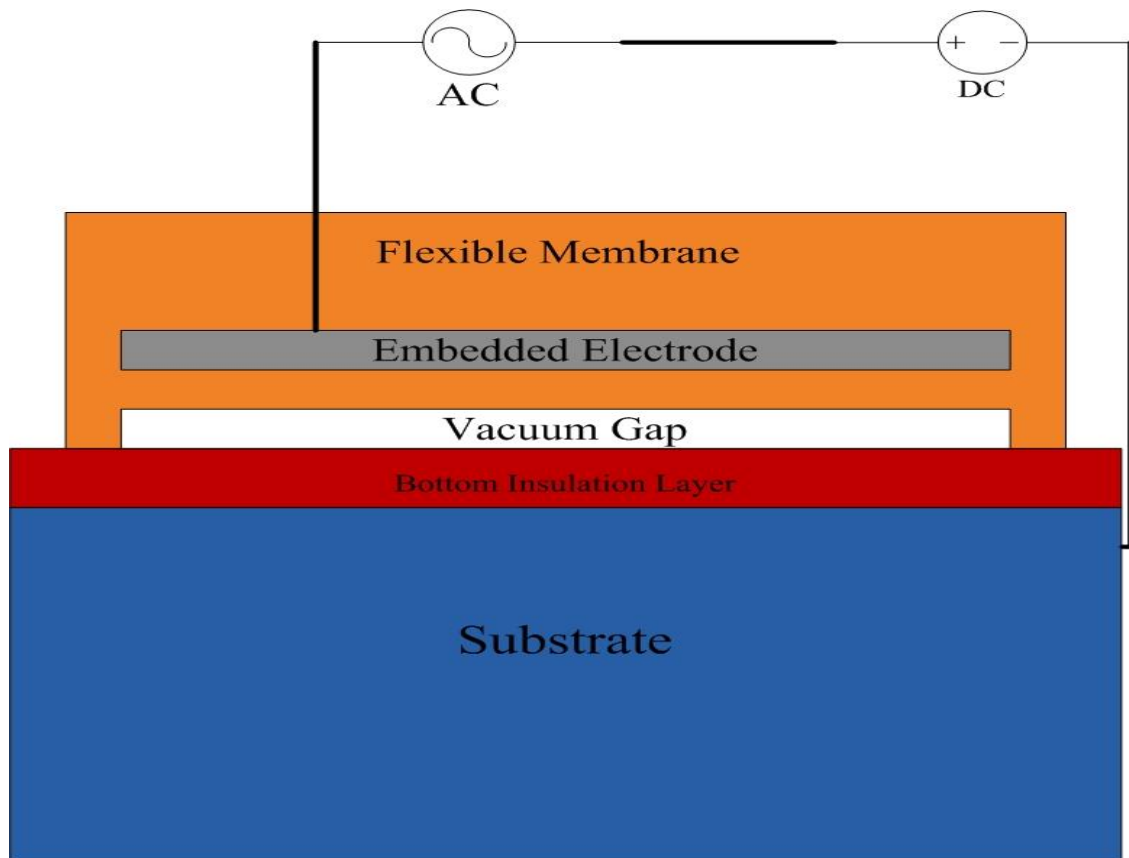
Figure 3-1: Cross section view of single CMUT cell (dimensions are not in the scale for better visualization)

the generated electrostatic force leads to the deflection of membrane toward substrate and then by applying an AC voltage, the membrane starts to oscillate and transmit the ultrasonic waves into the medium. In this operation mode, CMUT is used as transmitter. However, if a DC biased CMUT is subjected to ultrasound pressure waves, the incident waves eventuate in vibration of membrane leading to harmonic change in charge density of membrane and consequently the change in capacitance which results in AC output current. CMUT is acting as receiver in this operation mode.

Increasing the biased voltage will eventuate in pulling the membrane toward the substrate as it is illustrated in Figure 3-2.
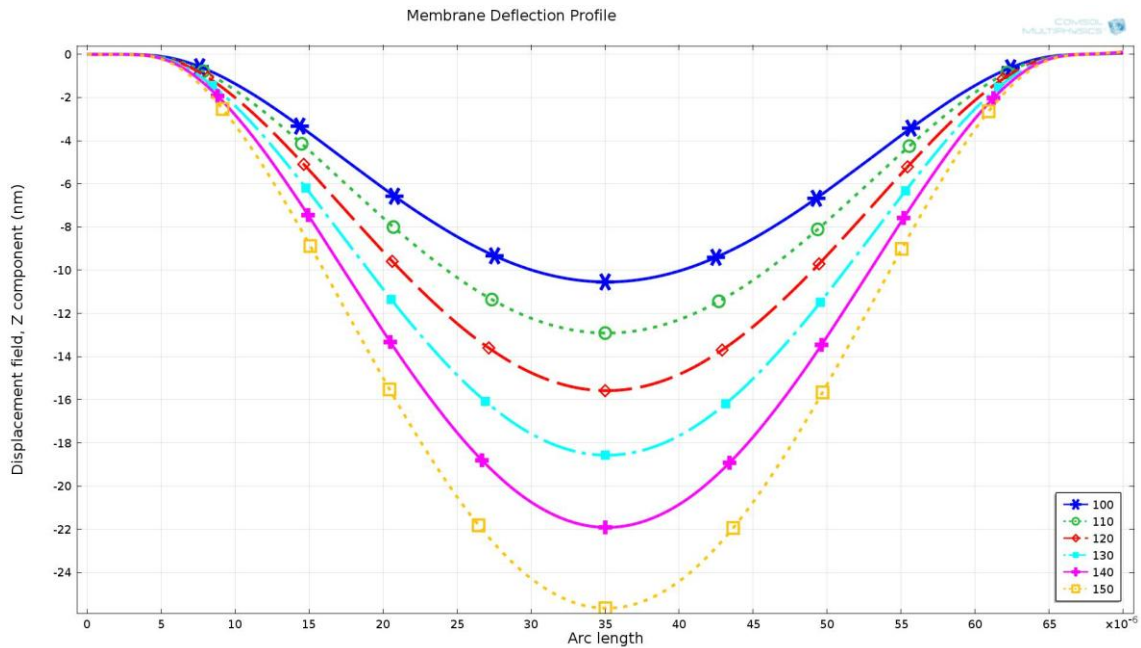
Figure 3-2: Deflection profile of CMUT membrane with 30µm radius for biased voltages between 100V and 150V

However, if the biased voltage further increased so that the mechanical restoring force couldn't tolerate the increased electrostatic force, the membrane will be pulled into collapse. The possibility of operating CMUT in collapse mode has been demonstrated [43-44].

3.2 Modeling of CMUTs

The development of models for the design of transducers is an essential study as brute force experimentation without tuning the device parameters can be cumbersome and time consuming and expensive. Models are usually based on the physics of the device, and expressed as relatively complex analytical equations. While optimization might be carried out analytically, the complexity of the models might usually require some simplifying assumptions, or even the use of numerical tools. Yet another practical method is to model the device behavior by means of a lumped electrical circuit, which then might be fed to a circuit simulator to sweep a wide range of parameters for optimization in a very efficient way. The validity of analytical and circuit models can be tested by the use of a very powerful numerical tool known as the Finite Element Method (FEM) which provides results as accurate as a physical experiment.

13

In equivalent circuit modeling, the mechanical parameters like mass, stiffness, and velocity are represented in electrical parameters and circuit components like capacitor, resistor or current[48].Physical phenomenon in many engineering applications might be explained in terms of partial differential equations, which can be solved analytically for simple systems. The equivalent circuit modeling of CMUTs begin by solving the differential equation of the membrane motion and then, calculating the mechanical impedance of the membrane [48]. On the other hand, the idea of dividing a particular shape into *finite elements* connected by *nodes* in Finite Element Analysis (FEA) makes it possible for analyzing complex systems and structures. FEA provides very accurate solutions for several problems including structural, thermal, electromagnetic, fluids, multi-body and coupled-field environments by using a numerical approach.

3.2.1 CMUT Analytical Modeling

The key parameters for the designing of a CMUT cell are the membrane thickness, diameter and the cavity height. These dimensions together with the magnitude of the DC bias voltage can be adjusted to obtain the transducer's center frequency, bandwidth, and transmit and receive sensitivity. Stiffness and size of CMUT cell membrane determine the central frequency where the small and stiff membranes result in high resonance frequency. The cavity depth (gap height) determines the maximum output pressure, the more membrane deflection, the more output pressure is. For a given center frequency, choosing the membrane size typically requires a tradeoff between bandwidth and sensitivity. For the CMUT cell designing purposes, one can use Finite Element Analysis (FEA) or CMUT circuit model for obtaining the device dimensions. Since it is time consuming using FEA and even CMUT circuit model; using analytical expressions is a quick start-up for obtaining the first draft dimensions and then further by FEA or CMUT circuit model.

For the deflections which are small in comparison with membrane thickness, modeling the circular CMUT membrane as spring-mass system is approved. The equivalent spring constant and mass can be formulated as Eq. 3-1 and Eq. 3-2[45]:

$$k_1 = \frac{192\pi D}{a^2} = \frac{16\pi E t^3}{a^2\left(1-v^2\right)}$$

Eq. 3-1

$$m = 1.84\pi a^2 \rho t$$

Eq. 3-2

where D, E, v, a, and t are plate flexural rigidity, membrane material's young modulus, Poisson's ration of membrane material, membrane radius, and thickness respectively. We can think of radiation impedance as plane–wave radiation impedance which is shown in Eq. 3-3.

$$R_b = \pi a^2 R_{rad}$$

Eq. 3-3

The undamped resonance frequency and mechanical quality factor could be extracted from these expressions. So for designing the CMUT cell using the following equations which express the thickness, membrane radius and gap height is beneficial [46].

$$t = 0.543\frac{R_{rad}Q}{\rho\omega_0}$$

Eq. 3-4

$$a = \frac{1.27}{\omega_0}\sqrt{\frac{QR_{rad}}{\rho^{3/2}}}\sqrt{\frac{E}{1-v^2}}$$

Eq. 3-5

where mechanical quality factor, Q, is expressed in Eq. 3-6.

$$Q = 5.43\frac{t_m^3}{a^2 R_{rad}}\sqrt{\frac{\rho\times E}{\left(1-\upsilon^2\right)}}$$

Eq. 3-6

In order to determine the gap height, the maximum DC biased and applied AC voltage of system could be converted in the term of pull-in voltage which effectively depends on gap height. The pull-in voltage could be express in term of gap height as Eq. 3-7.

$$V_{PI} = \frac{1.56}{a^2} \sqrt{\frac{E \times t_m^3 \times g_0^3}{\varepsilon_0 \left(1 - \upsilon^2\right)}}$$

<div align="right">Eq. 3-7</div>

Rearranging the Eq. 3-7 gives the gap in term of pull-in voltage.

$$g_0 = 1.87 \left(\frac{\varepsilon_0 V_{PI}^2}{R_{rad} Q \omega_0} \right)^{\frac{1}{3}}$$

<div align="right">Eq.3-8</div>

The first approach of designing CMUT cell is related to decide of resonance frequency. As it seems from Eq. 3-9 there are a lot of CMUT membrane radius and thickness whose values satisfy the criteria of operating the CMUT in constant resonance frequency.

$$\omega_0 = \frac{2.95 \times t_m}{a^2} \sqrt{\frac{E}{\rho \left(1 - \upsilon^2\right)}}$$

<div align="right">Eq. 3-9</div>

However, there are other parameters which should be taken into account. As the membrane radius increases, the bandwidth decreases due to the increasing the stiffness and mass. So, stiffer membranes have lower bandwidth in comparison with softer membranes operating in the same resonance frequency. Also the center of membrane can move above the relaxed position of it in stiffer (small bandwidth) membrane resulting in higher output pressure. It has been shown that for a fixed gap height and resonance frequency, applying 60% of collapse voltage will result in maximum output pressure [47].

3.2.2 Finite Element Method

A finite element method is a strong tool for modeling MEMS devices as well as CMUT. FEM is the most accurate for a number of reasons. It has the ability to incorporate the exact shape and size of the devices hence, all the nonlinear behavior of device could be modeled. For analyzing the CMUT array in immersion, CMOLSOL Multiphysics® and ANSYS® was used in this thesis. For analyzing the CMUT array, three physical domains were incorporated in the simulation domains: a) Electrostatic domain for modeling the applied voltage and calculating the capacitance and electrostatic force; b)

16

Mechanical domain for coupling the electrostatic force to this domain and studying the membrane deflections and other parameters; c) Acoustic domain for coupling the mechanical vibration to surrounded medium and study the generated output pressure.

For analyzing the CMUT array some assumptions are made. First, it is assumed that all the CMUT cells in array have identical behavior. Based on this assumption, CMUT array is simplified to a single CMUT cell. However, in order to incorporate the whole cells behavior, boundary conditions are adjusted so that the software considers it as a whole device. Second, it is assumed that the topology of placing the device in array is square placing rather than hexagonal topology for simplicity due to the difficulties of changing the orientation axis of simulation. Based on these assumptions, a 3-D CMUT structure is modeled in COMSOL.

Using analytical equations is the good start up for choosing the device parameters. After deciding about device dimensions, the second step in FEM simulation is Eigen-Frequency analysis of device to obtain the device first resonance frequency and adjust the dimensions if needed. Figure 3-3 shows the plate modes of CMUT membrane which used to find the CMUT resonance frequency.
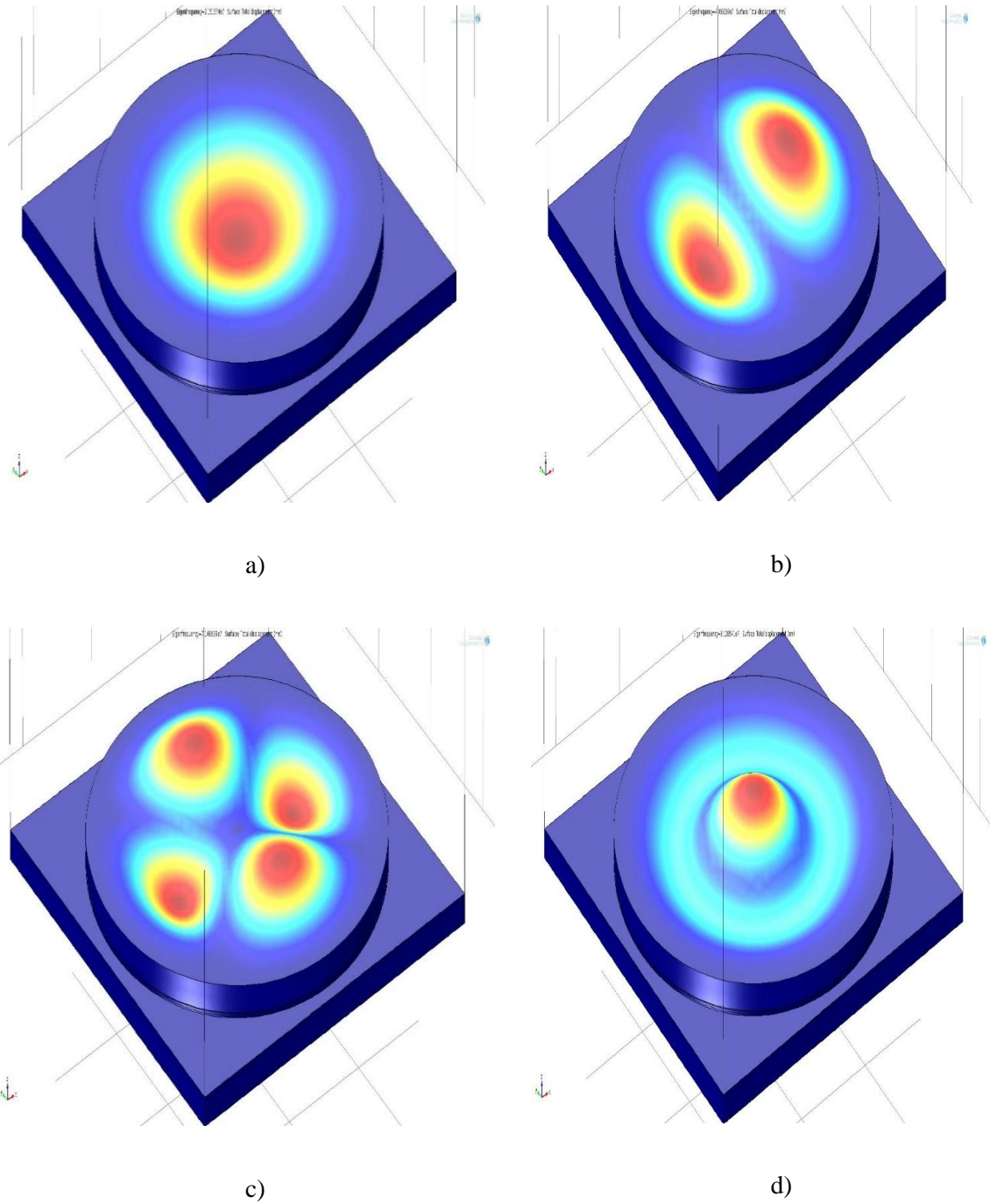
Figure 3-3: First 4 Modes of CMUT membrane.

The Eigen-frequencies are a) 21.13MHz b) 44.66MHz, c) 71.48 MHz, d) 81.28 MHz.

The dimensions of CMUT cell which are used to obtain the central frequency of 20MHz is listed in table 3-1.

Parameter	Description	Value
a	Membrane radius	20μm
ti	Bottom & top insulation layer	300nm
tg	Cavity height	100nm
tm	Membrane thickness	3μm
te	Embedded electrode thickness	100nm

Table 3-1: CMUT cell dimensions for operating in 20MHz

Silicon Nitride (Si_3N_4) and Gold (Au) are used as the membrane and electrode materials and the material properties are taken from COMSOL material library.

Another analysis which could be done for obtaining the device behavior is frequency-harmonic perturbation analysis.

Since 3-D FEA requires a relatively large mesh in this analysis, the quarter of the CMUT membrane is considered. In order to analyze the structure, symmetry boundary conditions are applied. The waveguide structure is used for modeling the surrounding fluid which is water (to mimic the human body.) The cell to cell distance is selected to be 5 μm due to the fabrication requirements. Also in frequency analysis there should be an absorbing boundary at the end of the waveguide so that could prevent the reflections which will affect the frequency response of system. In COMSOL Multiphysics®, Perfectly Match Layer (PML) could be used for introducing the absorbing boundary to the system. Also in order to model the CMUT in array, introducing the *periodic* boundary is the only way for modeling the CMUT in array. *Continuity periodic* boundary condition assumes that there are an infinite number of devices working identically around the system. Figure 3-5 demonstrates that the generated output pressure is 10.35 MPa when the transducer is driven by 100V bias and 80V AC voltage for a 20μm CMUT cell membrane.

19
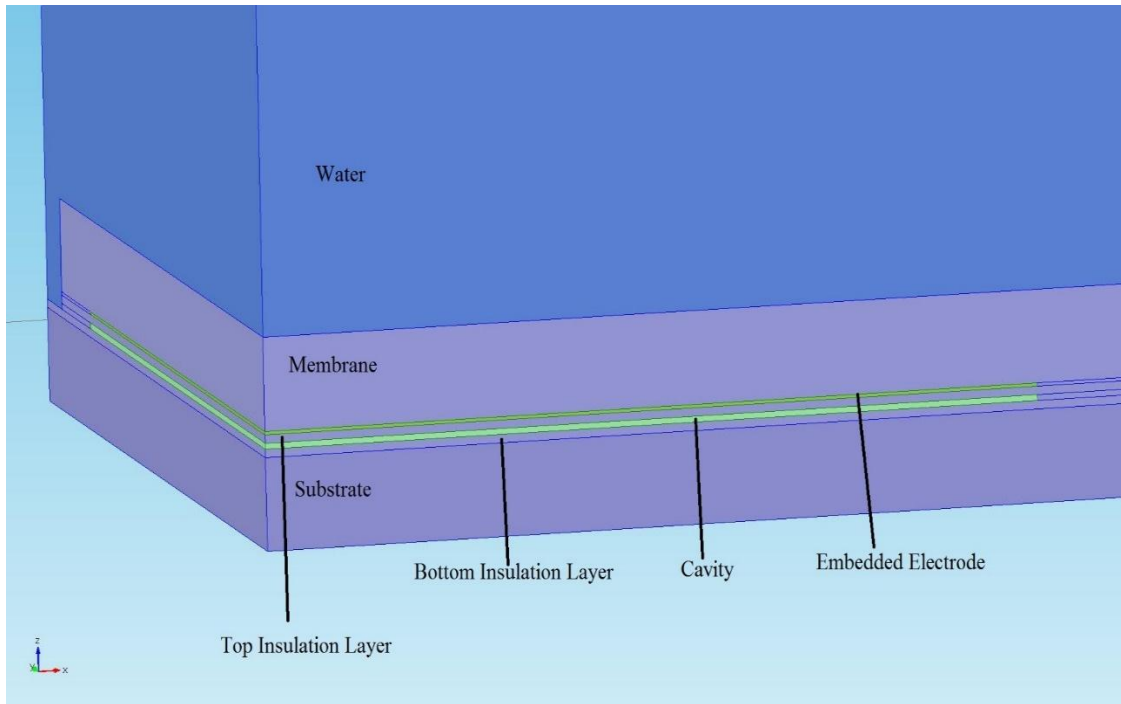
Figure 3-4: quarter structure of CMUT cell
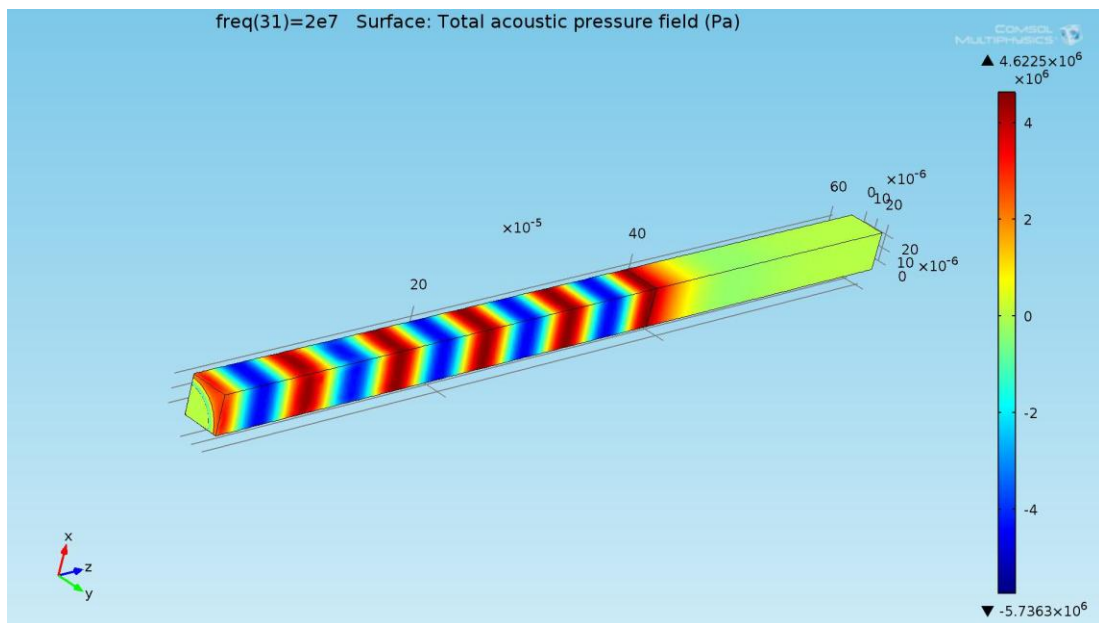
Figure 3-5: Generated 10.35 MPa peak-to-peak output pressure of CMUT array in immersion operating in 20MHz with radius of 20μm driven by 100V DC and 80V AC sources.

Also the frequency response of this system is examined and the result is shown in Figure 3-6
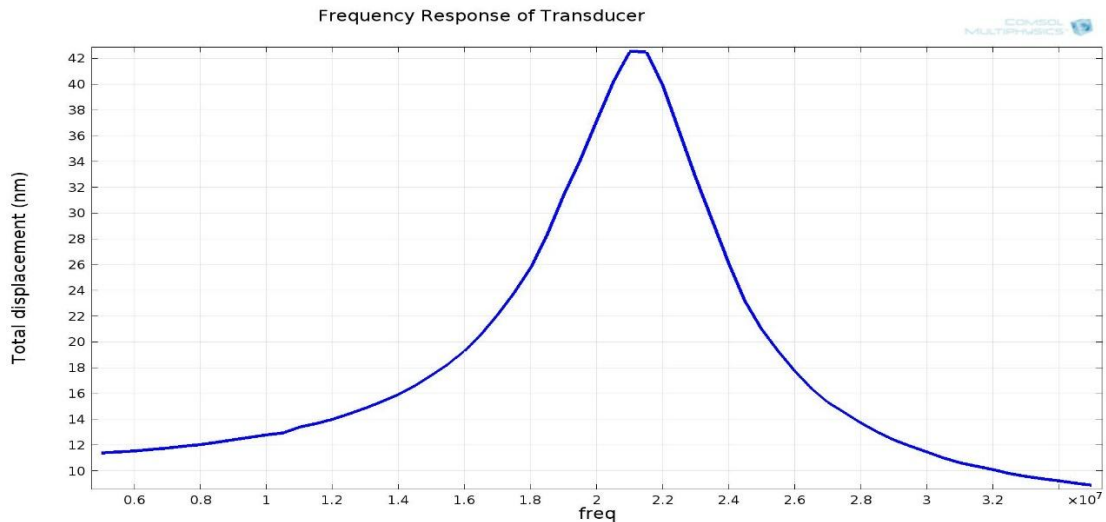
Figure 3-6: Membrane deflections for frequency ranges 5MHz-35MHz for CMUT cell with 20μm radius

Since this type of designed CMUT is stiffer one, the bandwidth of 4.7MHz which is smaller in comparison with other designs and is roughly equals to 25% fractional bandwidth, the center of membrane moved above the relaxed position resulting in high output pressure.

3.2.3 Equivalent Circuit Modeling

Mason's equivalent circuit model are generally used in modeling the CMUT which consists of series LC sections which L and C represents the mass and stiffness of membrane, respectively. When the device is immersed, it is necessary to consider the terminating radiation impedance in the equivalent circuit in order to represent the device behavior correctly. The radiation impedance of an aperture is determined by the particle velocity distribution across the aperture. The particle displacement and the velocity profile across circular clamped membranes are not uniform and can be very well approximated as [49]:

$$\upsilon(r) = (n+1)\upsilon_{avg}\left[1-\frac{r^2}{a^2}\right]^n \text{ for } r < a$$

Eq. 3-10

where a is the radius of the radiator, r is the radial position, v_{avg} is the average velocity and n is an integer that determines the structure of the profile. Case $n = 0$ is dedicated to

21

the velocity profile of a rigid piston and $n = 2$ accurately matches to the profile of a clamped membrane which is the case for CMUT membrane.
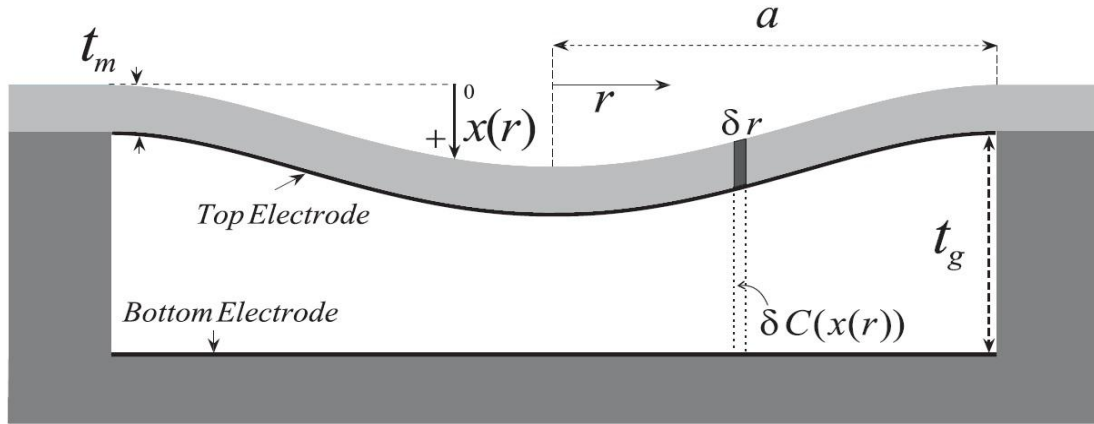
Figure 3-7: Cross-section view of CMUT geometry [50]

If a biased voltage is applied to CMUT electrode and driven by an AC voltage such that $V(t)= V_{DC} + V_{AC}(t)$; the total electrostatic force acting on membrane can be expressed as [52]:

$$F_{tot} = \frac{C_0 V^2(t)}{4t_g} \left[\frac{t_g}{t_g - x_p(t)} + \frac{\tanh^{-1}\left(\sqrt{x_p(t)/t_g}\right)}{\sqrt{x_p(t)/t_g}} \right]$$

Eq. 3-11

where $x_p(t)$ is the peak displacement at the center of the membrane, and C_0 is the initial capacitance of CMUT membrane when no deflection is proposed.

The current flowing through electrodes of CMUT could be analyzed by evaluating the derivative of stored charge on membrane which yields:

22

$$I_{tot} = I_{cap}(t) + i_c(t) = C_0 \frac{dV(t)}{dt} + C_0 \frac{dV(t)}{dt}\left[\frac{\tanh^{-1}\left(\sqrt{x_p(t)/t_g}\right)}{\sqrt{x_p(t)/t_g}} - 1\right]$$

<div align="right">Eq. 3-12</div>

where $I_{cap}(t)$ is the capacitive current and $i_c(t)$ is induced by membrane motions and is referred as *velocity current* which also could be expressed as

$$i_{vel}(t) = \frac{C_0 V(t)}{2x_p(t)} \frac{dx_p(t)}{dt}\left[\frac{t_g}{t_g - x_p(t)} - \frac{\tanh^{-1}\left(\sqrt{x_p(t)/t_g}\right)}{\sqrt{x_p(t)/t_g}}\right]$$

<div align="right">Eq. 3-13</div>

As it is illustrated in Figure 3-8, in the electrical part of the equivalent circuit which is left side of the circuit, C_0 is the shunt input capacitance of the CMUT, i_c is the nonlinear component of the capacitive current, and i_{vel} is the motion-induced current according to Eq. 3-29. The mechanical part of the circuit is on the right-hand side. The electrical attraction force, f_R, and the force exerted by the atmospheric pressure, F_b are represented by voltage sources. The mass and the stiffness of the plate are represented by an inductor, L_{Rm}, and a capacitance, C_{Rm}, respectively. The parameter N represents the number of cells in an array and provides scaling to the equivalent circuit. As it is appears from Eq. 3-29, the behavioral current and voltage sources in the circuit require the instantaneous peak displacement of the plate, x_P, as a parameter which is represented by dividing the restoring force of the plate, F_{Rm}, by the plate stiffness.
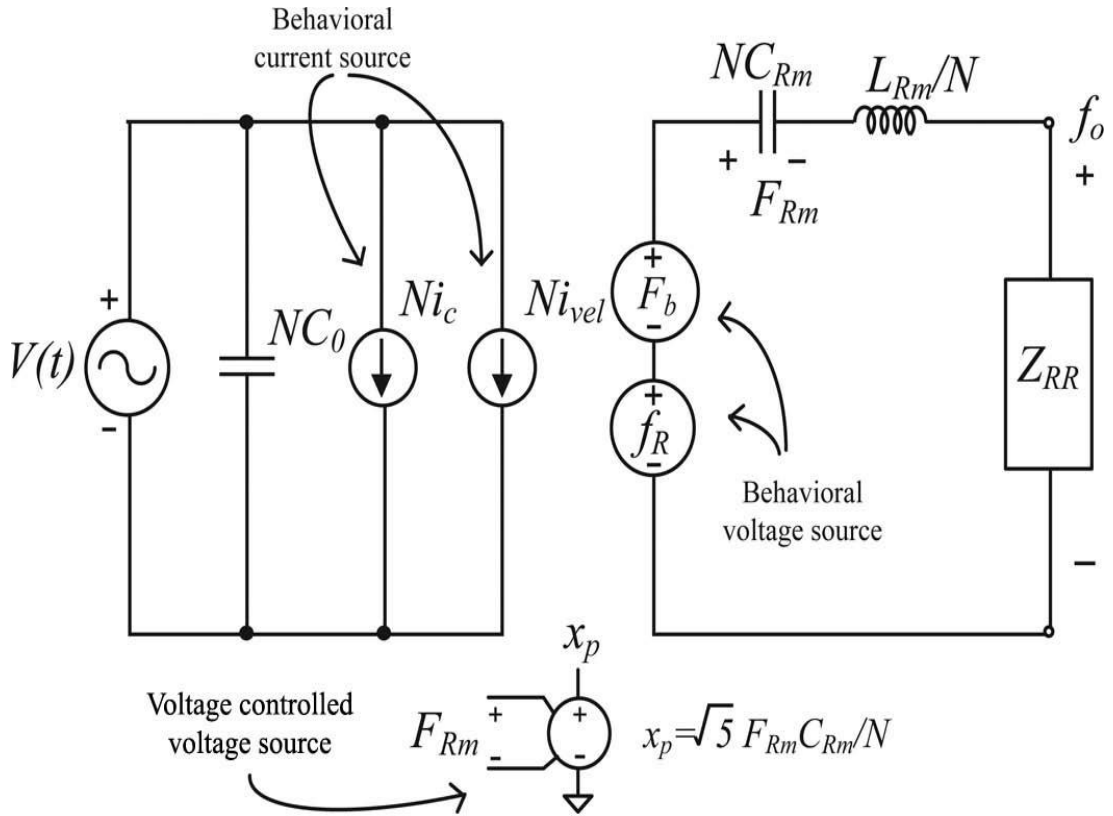
Figure 3-8: Electrical Circuit model of Capacitive Micromachined Ultrasound Transducer (CMUT) array [9]

The electrical attraction force, f_R, could be calculated by

$$f_R(t) = \frac{C_0 V^2(t)}{4x_p(t)} \left[\frac{t_{ge}}{t_{ge} - x_p(t)} - \frac{\tanh^{-1}\left(\sqrt{x_p(t)/t_{ge}}\right)}{\sqrt{x_p(t)/t_{ge}}} \right]$$

Eq. 3-14

where t_{ge} is the effective gap height and expresses as

$$t_{ge} = t_g + \frac{t_i}{\varepsilon_i}$$

Eq. 3-15

The force exerted by atmospheric pressure is formulated as

$$F_b = \frac{\sqrt{5}}{3} P_0 \pi a^2$$

Eq. 3-16

The membrane mass which is represented by inductance is
24

$$L_{Rm} = \rho t_m \pi a^2 \qquad\qquad \text{Eq. 3-17}$$

and the capacitor stands for stiffness of membrane

$$C_{Rm} = 1.8 \left[\frac{(1-\sigma^2)a^2}{16\pi Y_0 t_m^3} \right] \qquad\qquad \text{Eq. 3-18}$$

where σ and Y_0 are the Poisson's ratio and Young's modulus of the plate material, respectively.

Since it is very time consuming process for optimizing the device parameter using FEM simulation, the equivalent circuit model is preferred over the finite element analysis and the results of circuit model is in good agreement of FEM results. However, modeling the radiation impedance plays a key role in accuracy of circuit model.

4. Optimization of the Pulse-Echo Response of a CMUT Transducer

In the study of the CMUT, scientists have been optimizing various properties of the transducer such as gain-bandwidth product, output pressure, and input sensitivity. A medical imaging system uses the same transducer for insonification and for listening to the return echo. Consequently, a more meaningful figure-of-merit would be the overall pulse-echo response of the system. This work analyses the pulse-echo response of the CMUT transducer to tune the device parameters so that, (i) the return echo amplitude is maximized, and (ii) the signal-to-noise ratio (SNR) is maximized.

Figure 4-1: Layout of the CMUT ring array: Top view (left), detail (right).

The analysis presented in this chapter is based on a case study. For a particular imaging device, a high frequency (20 MHz) 4-element ring array was required. Various other design requirements lead to a device with radius 1.75 mm, for which the outer ring is as small as 234 µm in thickness (Fig.4-1). Construction of such a device using pi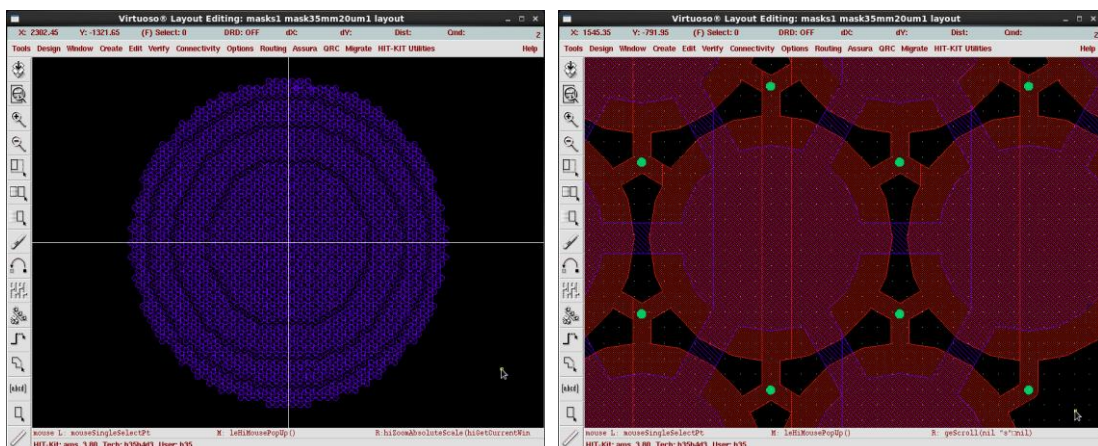ezoelectric transducers is extremely difficult, especially due to the difficulty in manufacturing such small structures, and the precision required for the matching layers. Due to the advantages of Capacitive Micromachined Ultrasound Transducer (CMUT) over piezoelectric transducer, such as being manufactured using standard lithography techniques (so that fine structures can be easily manufactured) and providing higher bandwidth especially in high frequency ranges, designing the transducer with CMUT is preferred.

The first step in designing the CMUT transducer is determining device dimensions based on the target operation frequency. As shown by Eq.3-9, membrane's material properties such as Young modulus and Poisson's ratio, membrane radius, and thickness affect the operation frequency. The membrane material is conventionally chosen as Silicon Nitride (Si_3N_4) due to superior material properties. Consequently, variable device parameters are reduced to membrane thickness and radius, and gap height. Since the operation frequency is fixed, the radius and thickness become dependent variables. As the bandwidth of CMUT depends on the stiffness and mass of membrane, increasing the radius results in bandwidth reduction. However, a transducer with a thick membrane has higher output efficiency. Another step in designing the CMUT is the gap height. According to Eq. 3-7, gap height determines the collapse voltage. It is suggested that the electric field in the gap should be with the strength on the order of 10^8V/cm or higher [53]. Also since the gap height limits the maximum membrane deflection and output pressure of CMUTs, this parameter will be chose so that meets the requirements of CMUT device. For example, in High Intensity Focused Ultrasound (HIFU) applications, it is desired to have large output pressure. Hence, CMUTs in HIFU applications have larger gap height.

For the optimization study that is the subject of this thesis, the following method is adopted: for the particular case study, two sets of membrane radius and thickness are determined. The DC bias voltage is swept from 0 Volts to the collapse voltage and for

27

each voltage the maximum applicable AC voltage is determined by monitoring the membrane deflection and keeping it less than the gap height.

4.1 Circuit Model for Optimizing the Pulse-Echo Response

The circuit simulations used for the optimization study was based on the model suggested by Hayrettin Koymen [38]. We make the following assumptions in the model: although the transducer has finite dimensions, the number of CMUT cells is large enough to make the assumption that there are an infinite number of cells. This is important in determining the radiation impedance of the transducer. Calculations will reveal that this assumption is reasonably accurate as cells surrounded by even a limited number of cells "think" that they are in an infinite field. In the circuit model of Fig.4-7, there are separate circuits for the pulse and echo part of the simulations. The pulse part is terminated by the radiation impedance of the medium. The output pressure is coupled back to the receiver circuit as if generated by a source of output impedance identical to the radiation impedance. The amplitude is scaled by the coverage ratio of the CMUT cells: output pressure is measured on the CMUT membrane but as the cell does not entirely cover the surface the pressure of the eventually created plane wave will have a lesser amplitude.

The radiation impedance of the CMUT depends on the number, spacing and arrangement of the cells. We start the analysis by first computing the radiation impedance of the transducer in consideration.

The radiation impedance of a CMUT defines how the membrane vibration couples to the surrounding fluid, and vice versa. In vacuum, this parameter will be zero, as there will be no fluid through which a pressure wave can propagate. In air, this parameter will exist, but will be very small because ultrasonic pressure waves do not propagate efficiently in such low density mediums. In water and similar fluids (e.g. blood), the radiation impedance has a significant effect on the frequency response of system and must be considered carefully.

Radiation impedance of a rigid circular piston in infinite baffle could be the simplest approximation for radiation impedance of a CMUT array. Figure 4-2 depicts this

radiation impedance when the medium is water. This model assumes that the entire membrane surface vibrates with a uniform velocity which is the case for piston vibrations.

As the frequency increases, the mode shapes of a plate are generated. Thus, the assumption of uniform velocity of membrane surface will no longer be valid and for reasonable accuracy, the piston model is not sufficient for modeling CMUT radiation [51].
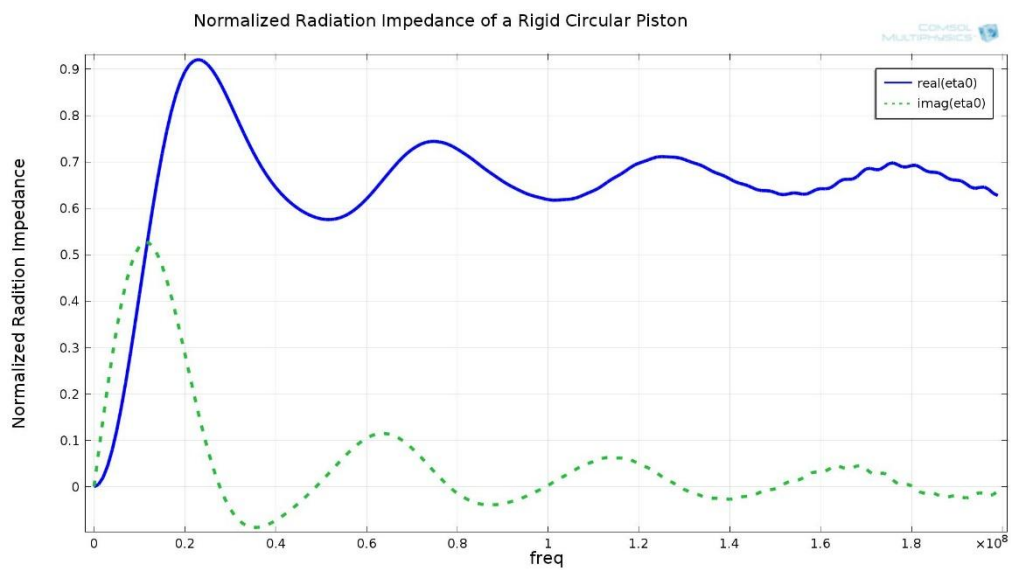
Figure 4-2: Normalized radiation Impedance of a rigid circular piston analyzed between 0-100MHz

Several researchers studied the radiation impedance of CMUT array in immersion [39, 52]. Their analytical approaches are in agreement with depicted results of device performance. Muhammed N. Senlik et al. [39] analyzed the radiation impedance mathematically and FEM simulation results for real part of radiation impedance was introduced. This thesis analyzed the radiation impedance of CMUT array in immersion by analytical and FEM approaches. The functions and constants pertain to radiation impedance in [39] was coded in MATLAB® and also FEM simulation using both ANSYS® and COMSOL Multiphysics® is done for studying the behavior of medium and examining the imaginary part of radiation impedance. As it is demonstrated by

29

Figure 4-3 shows the radiation impedance of CMUTs with a=22 μm. Although there is a peak in real part of radiation impedance however, the same peak for imaginary part of it is seen for that operation frequency. We therefore propose that the transducer should be operated at a lower *ka* product, i.e. a transducer of smaller radius is expected to be more appropriate to be operated at 20 MHz.
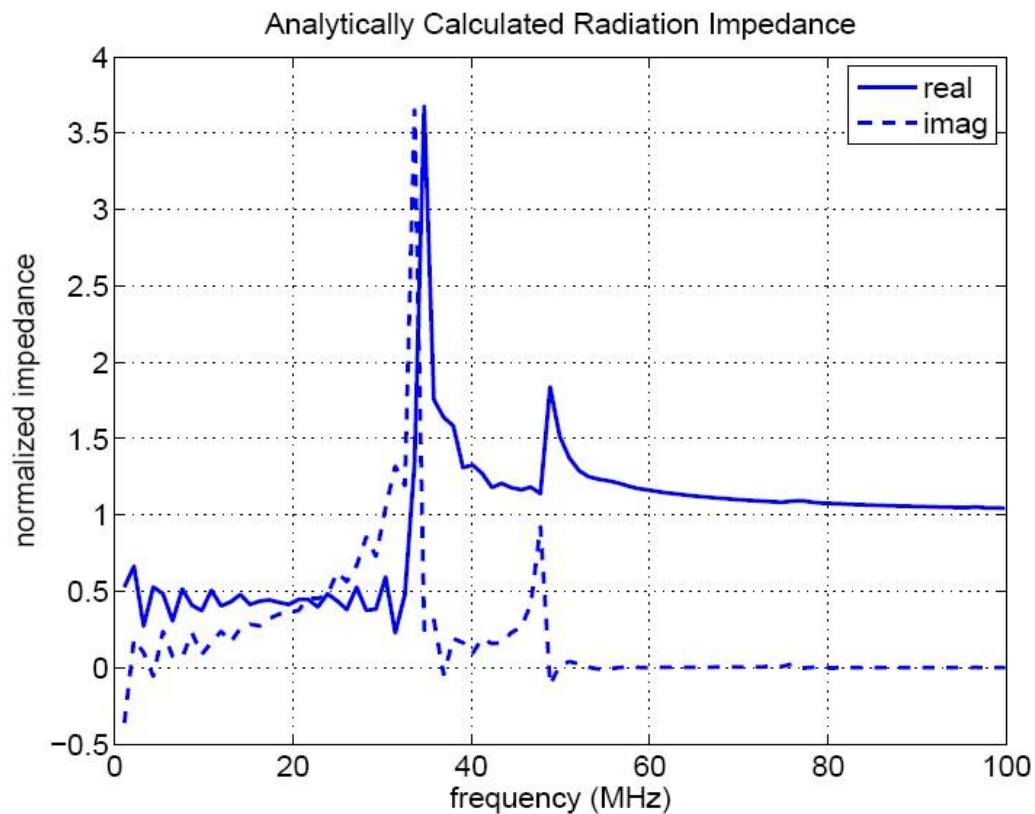
Figure 4-3: Analytically calculated normalized radiation impedance of CMUT array in immersion using the expressions provided in [39]

The radiation impedance of CMUT array is studied using FEM simulation for CMUT with radius of 22μm and 15μm and compared with analytical results. In analytical expression, a CMUT array of 11×11 is coded and self and mutual radiation impedances are examined. It is clear that this size of array is enough to think of the CMUT cell which is located at the center of the array, could model the infinite CMUT cell which this assumption is used in FEM simulation by introducing the continuity boundary conditions. (Figure 3-5). Since 11×11CMUT array size could model the infinite

environment of central located CMUT cell, it is applicable for CMUT array size with more than 11×11 cells.
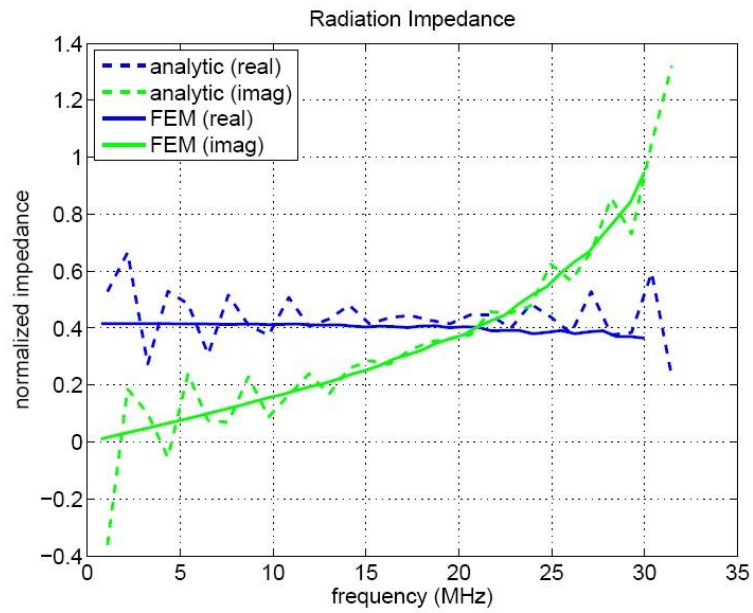
Figure 4-4: Analytical and FEM based simulation results for CMUT array with 22µm radius
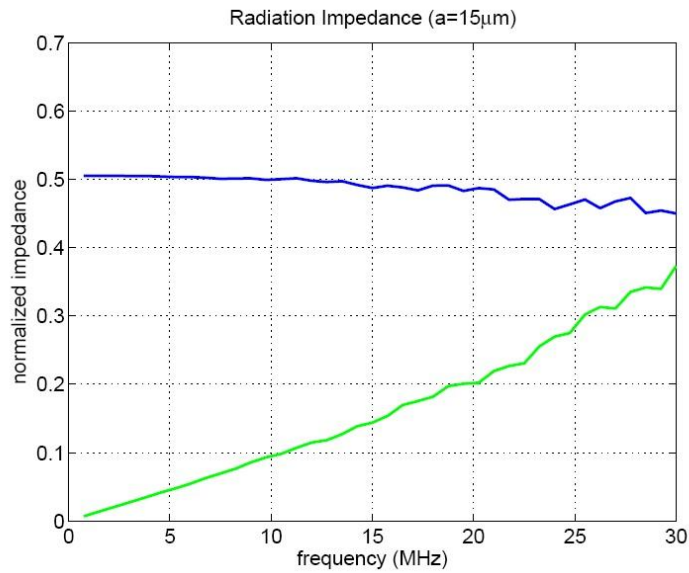
Figure 4-5: FEM based simulation results for CMUT array with 15µm radius

So it is clear that in circuit model, representing the radiation impedance with resistor is not enough. For proper modeling, one should include the imaginary part of radiation

31

impedance in circuit model by putting a series inductance with resistor. Since the frequency analysis range in circuit simulator is studied between 1Hz-30MHz, an inductance is a good representative of imaginary part of radiation impedance.

For physical description of this new model, as the frequency increases, each CMUT cell acts like point source and consequently, there will be large numbers of wavelength between two CMUT cells which means they become far away from each other in frequency domain even though they have located close to each other in time domain. In this case, waves between two adjacent CMUT cells will become standing waves which are not propagating. Consequently, these waves eventuate in increasing the mass between CMUT cells in array and the component models the mass in equivalent circuit model is an inductor.

In all optimization studies the return signal is measured as the AC current that flows over the DC bias source. In an actual implementation, the AC return signal is decoupled from the bias source and is fed into a trans-impedance amplifier, as the CMUT has relatively large output impedance. Consequently, the DC source acts as the input of the trans-impedance amplifier, and by these means, noise contribution that is only due to the radiation impedance can be observed.

4.2 Optimization of the Return Echo Amplitude

Implementing the radiation impedance in LTSpice circuit simulator enabled us to optimize the device parameter of CMUT array with size of 1mm×1mm designed for operation in 20MHz frequency. Two CMUT array is designed for this purpose; one with radius of 20µm and other one with 15µm radius. Table 4-1 shows the device parameters.

32

Parameter	Description	Value	
a	Membrane radius	20μm	15 μm
ti	Bottom & top insulation layer	300nm	300nm
tg	Cavity height	100nm	100nm
tm	Membrane thickness	3.13μm	2μm
te	Embedded electrode thickness	100nm	100nm

Table 4-1: CMUT cell parameters for operating in 20MHz pulse-echo medical imaging system

In order to fair judge optimization, gap heights of device kept constant. However, since membrane thicknesses and consequently collapse voltages of CMUTs changed, the applied DC and AC voltage is adjusted so that the center of membrane reaches to the bottom of cavity.

Figure 4-6 shows the whole system for 20MHz pulse-echo ultrasound imaging. The upper side of circuit model is dedicated to transmit part of CMUT array and lower one is assigned for receiving mode.
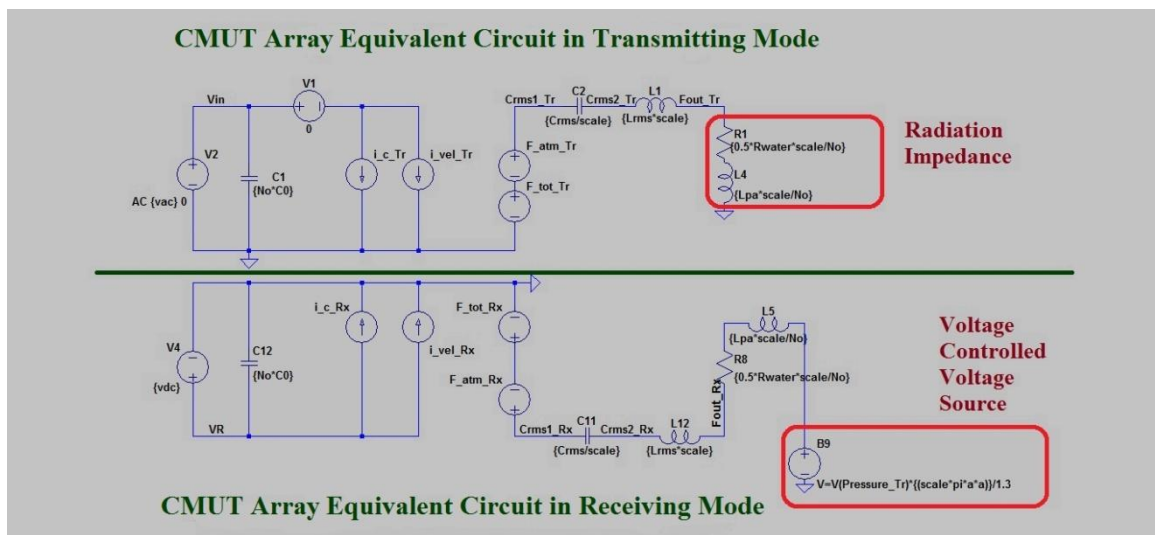
Figure 4-6: Equivalent circuit model of CMUT array operating in 20MHz for pulse-echo imaging system implemented in LTSpice [9].

The sub-circuits are used to generate the required parameter values such as membrane deflection or output pressure or for generating the controlling signals of system.
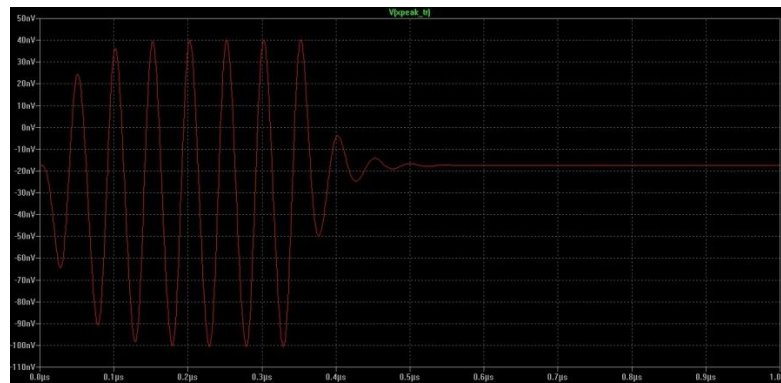
Figure 4-7: Membrane deflection of 20µm radius biased by 120V and driven with 7 cycles AC source.
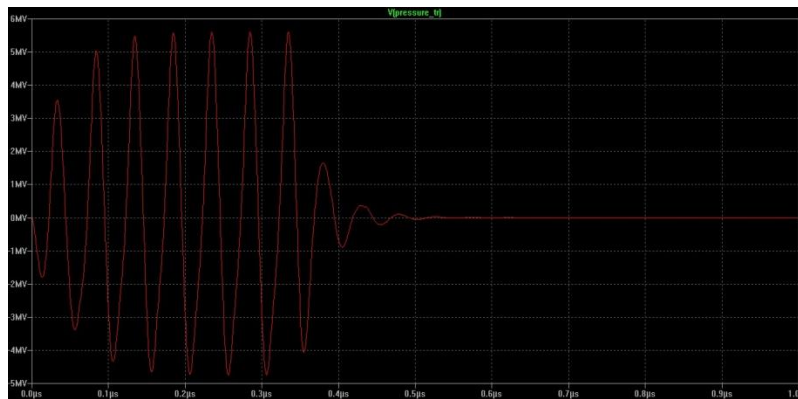
Figure 4-8: Transmitted pressure of CMUT with membrane radius size of 20µm biased by 120V and driven with 7 cycles AC source.
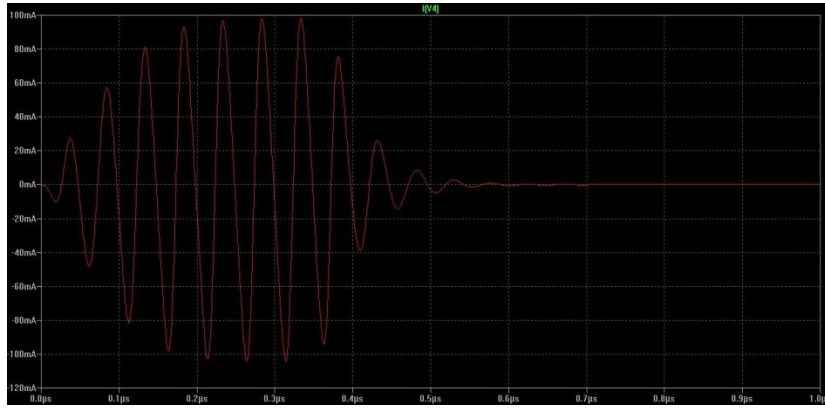
Figure 4-9: Pulse-echo response of CMUT array system as output current for membrane
radius size of 20μm biased by 120V and driven with 7 cycles AC source.

Figures 4-7, 4-8, 4-9 demonstrate the pulse-echo response of CMUT array system
operating in 20MHz for membrane radius size of 20μm which is biased by 120V DC
and driven by 7 cycles of AC voltage. The required information regarding the parameter
values of two sets of CMUT array is illustrated in tables 3-3 and 3-4.

$V_{DC}(V)$	$V_{AC}(V)$	Transmit Pressure P-P (MPa)	Receive Pressure P-P (MPa)	Output Current (mA)
90	125.75	11.04	6.73	78.39
100	112.50	10.74	6.41	91.25
110	99.40	10.37	5.84	104.34
120	86.50	9.85	4.86	117.16
125	80.75	9.53	4.37	120.17
130	74.00	8.95	3.58	124.53
135	65.00	8.13	2.71	118.79
140	54.00	6.95	1.68	108.00
150	23.00	3.00	0.327	51.80

Table 4-2: Device performance of pulse-echo system of CMUT array with 15μm
membrane radius

35

V_DC(V)	V_AC(V)	Transmit Pressure P-P (MPa)	Receive Pressure P-P (MPa)	Output Current (mA)
90	99.50	11.00	10.62	137.87
100	88.50	11.03	10.25	161.81
110	78.75	10.73	9.30	184.65
120	70.25	10.25	7.82	199.61
125	66.50	9.92	6.88	202.98
130	63.50	9.65	5.87	202.38
135	60.00	9.16	4.82	197.06
140	56.50	8.61	3.72	185.95
150	48.50	6.98	1.64	147.57

Table 4-3: Device performance of pulse-echo system of CMUT array with 20µm membrane radius
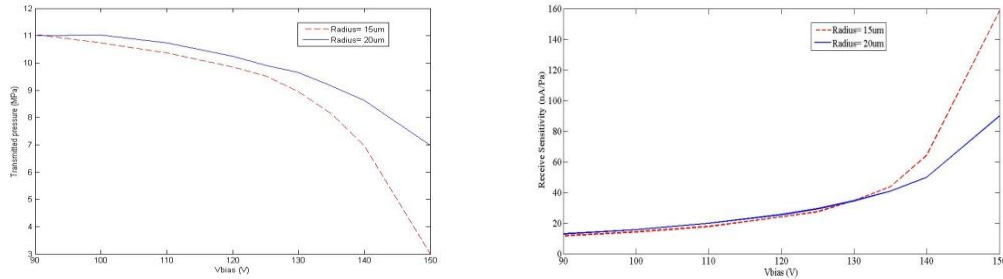
Figure 4-10: Transmit pressure (left) and receive sensitivity (right) of the transducers with a=15um and a 20um.

Figure 4-10 shows the results in Table 4-2 and 4-3 in graphic form. The transmit pressure decreases with increasing bias as the membrane has less distance to move. The receive sensitivity is calculated by dividing the output current by the input pressure. This sensitivity, as expected, improves with bias.

Figure 4-11 depicts the output current as a function of bias voltage. As bias voltage acts oppositely on output pressure and input sensitivity, an optimal value for the pulse-echo response was anticipated. This figure shows that there is indeed such an optimal point, which corresponds to approximately 70% of the collapse voltage.
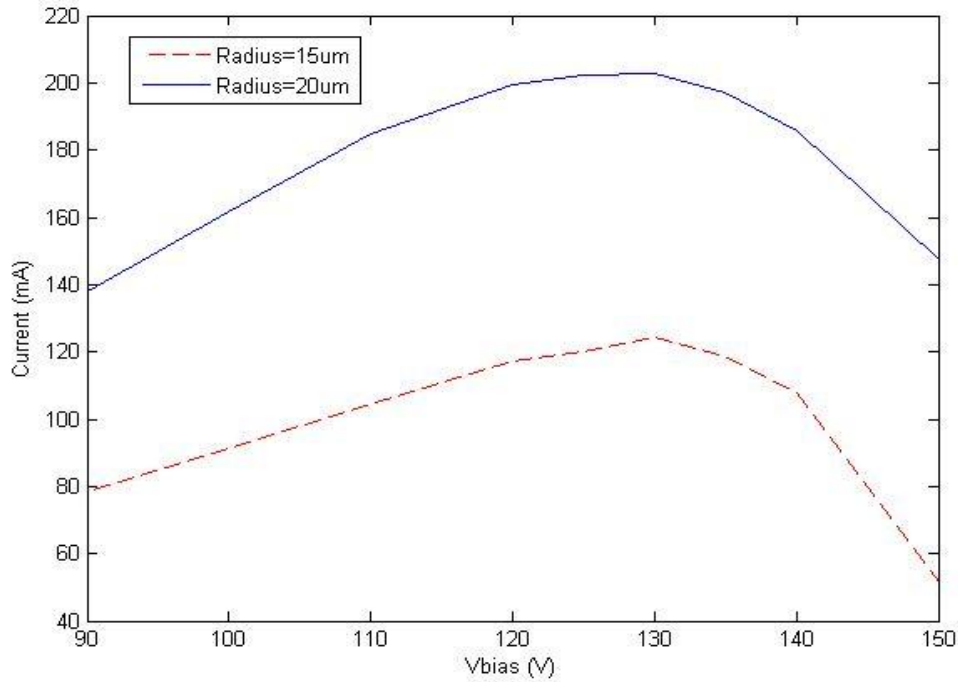
Figure 4-11: Pulse-echo response of CMUT array systems for membrane radius of
15µm and 20µm

4.3 Optimization of the Signal-To-Noise Ratio

One important parameter in the design of high frequency medical ultrasound imaging transducers is the signal-to-Noise ratio (SNR). The goal of this thesis is to determine the optimal point of CMUT array by considering the SNR. Signal-to-Noise ratio is a measure used in science and engineering that compares the level of a desired signal to the level of background noise. It is defined as the ratio of signal power to the noise power, often expressed in decibels. The noise source in this analysis is considered to be the thermal noise of the immersion medium. With a simplifying assumption, the noise source is taken as the real part of the radiation impedance. This is a valid argument for a single transducer, however, for the CMUT the mutual impedance effects should be also considered.

The noise analysis is studied in LTSpice circuit simulator for the whole pulse-echo system implemented as Figure 4-6. For fair comparison, both transducers are assumed

37

to have the same area. Again, it is assumed that both CMUT array sets of membrane sizes of 15µm and 20µm are biased by the same amount of voltage and AC signal applied so that the membrane center is not reached to the substrate. So the Biased voltages and AC driven voltages are the same as listed in table 3-3 and table 3-4 dedicated to membrane sizes of 15µm and 20µm, respectively. The Noise analysis is done for the spectrum range between 100Hz-35MHz due to the fact that radiation impedance which has been implemented in equivalent circuit model is valid up to 35MHz as Figures 4-4 and 4-5 demonstrate. The device is assumed to operate in room temperature for both CMUT array sets.

Output noise power and output power (desired signal) is analyzed for the biased voltages between 90V-150V. The simulation results are listed in tables 4-4 and 4-5.
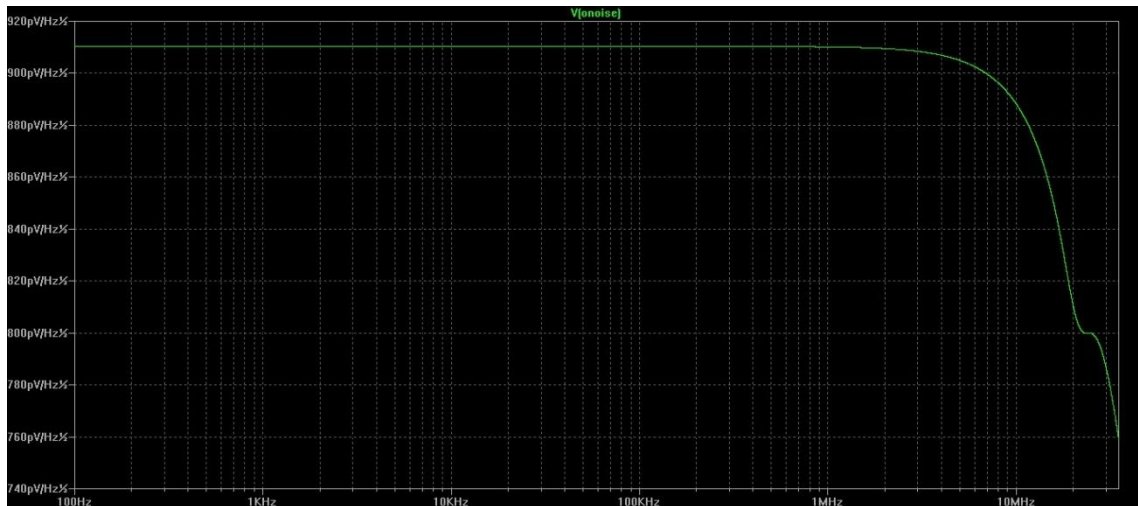

Figure 4-12: Output noise voltage of CMUT array in immersion analyzed for membrane radius sizes of 20µm

Figure 4-12 shows the output noise voltage of CMUT array for radius size of 20µm which is biased at 100V DC and analyzed between 100Hz-35MHz frequency range. Taking the integral of whole spectrum (100Hz-35MHz) for squire of noise voltage will give us the noise power.

V_{DC}	90	100	110	120	125	130	135	140	150
RMS Output Noise Power$\times10^{-15}$	4.614	4.588	4.557	5.119	4.468	4.432	4.386	4.325	4.072
Output Power (mW/Ohm)	13.012	17.044	21.147	24.990	33.733	37.213	38.407	36.564	16.602
SNR (dB)	124.537	125.696	126.665	127.426	128.7786	129.240	129.423	129.269	126.103

Table 4-4: Signal-to-Noise ratio for frequency ranges between 100Hz-35MHz of CMUT Array in Immersion for membrane radius size of 15µm

V_{DC}	90	100	110	120	125	130	135	140	150	160	165
RMS Output Noise Power $\times10^{-15}$	4.255	4.224	4.188	4.147	4.123	4.098	4.034	3.990	3.875	3.666	3.325
Output Power (mW/Ohm)	30.120	37.637	45.455	53.689	58.131	63.755	79.514	87.150	100.57	60.91	1.49
SNR (dB)	128.49	129.396	130.355	131.121	131.491	131.918	132.947	133.39	134.14	132.2	116.51

Table 4-5: Signal-to-Noise ratio for frequency ranges between 100Hz-35MHz of CMUT Array in Immersion for membrane radius size of 20µm

As it is depicted by Figure 4-13, output noise power of CMUT array with membrane radius of 20µm is lower than that of for 15µm. At first look, one can be alleged that due to the bigger radius of CMUT in 20µm, the area of CMUT which collects the noise is bigger and the output noise current should be larger than the other. However, the reason that it is lower than 15µm radius size of CMUT array is due to the flexural rigidity.
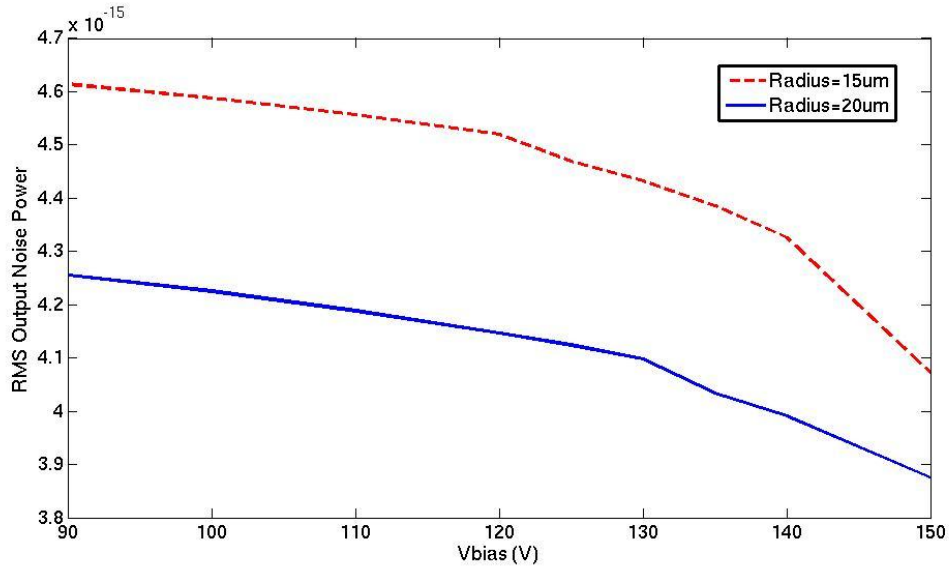
Figure 4-13: RMS Output Noise Power of CMUT array in immersion for ultrasonic
pulse-echo imaging purposes analyzed for membrane radius sizes of 15μm and 20μm

Flexural rigidity is defined as the force required to bend a non-rigid structure to a unit
curvature or it can be defined as the resistance of structure against the bending force.

$$D = \frac{Y_0 \times t_m^3}{12(1-v^2)}$$ Eq. 4-1

According to Eq.3-35, since CMUT array with membrane radius of 20μm is thicker
than the other, the flexural rigidity (D) of it is also larger. Since noise sources are equal
for both designs, the one which has larger *D*, less affects by noise and has lower output
noise current.
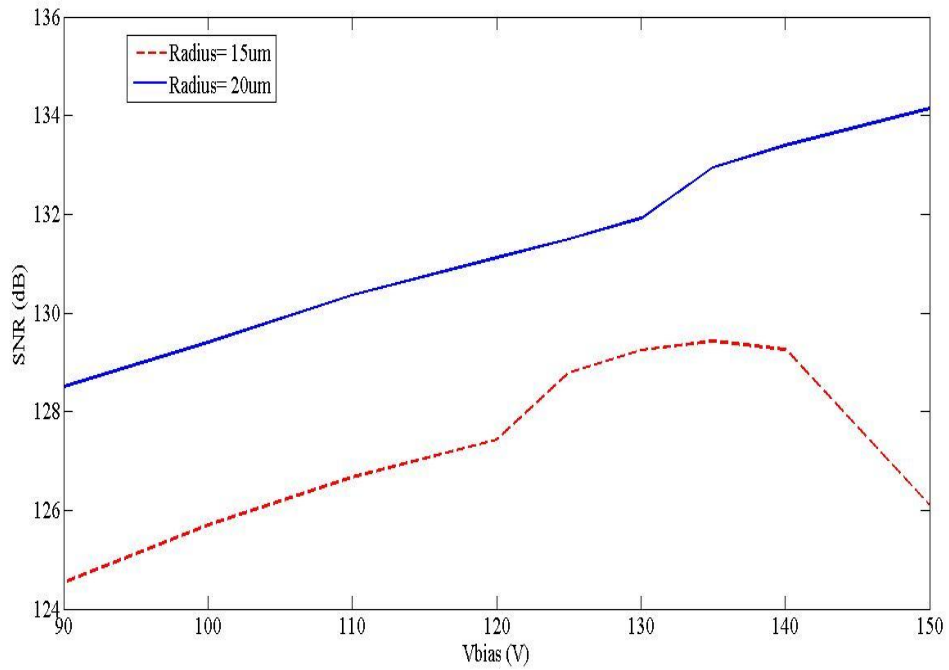
Figure 4-14: Signal-to-Noise ratio for frequency ranges between 100Hz-35MHz of CMUT Array in Immersion for membrane radius sizes of 15µm and 20µm
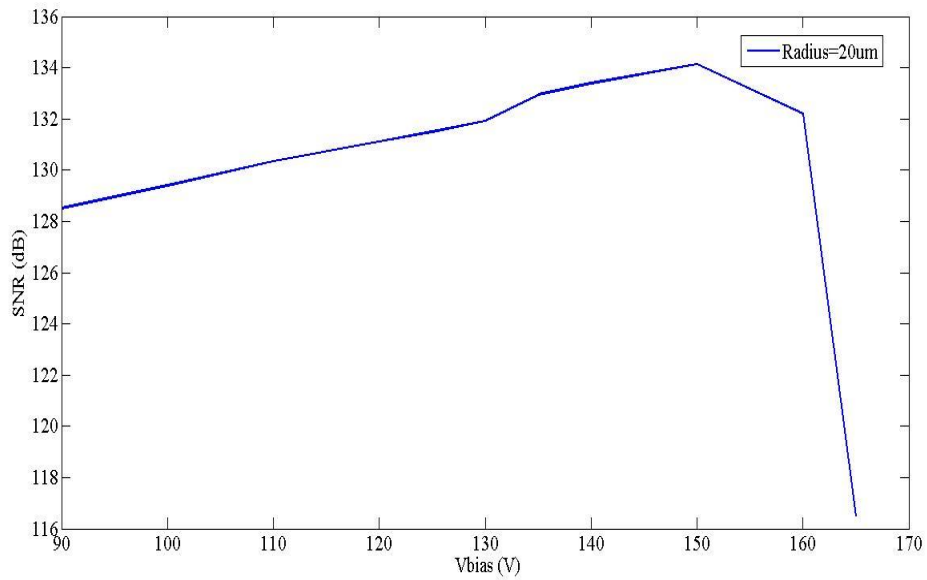
Figure 4-15: Signal-to-Noise ratio for frequency ranges between 100Hz-35MHz of CMUT Array in Immersion for membrane radius sizes of 20µm

41

After finding the output current and output noise current, finding the Signal-to-Noise ratio can be studied by using the following equation.

$$SNR_{dB} = 10\log_{10}\left[\left(\frac{A_{signal}}{A_{noise}}\right)^2\right] = 20\log_{10}\left(\frac{A_{signal}}{A_{noise}}\right)$$

Eq. 4-2

where A is dedicated to Voltage or Current signals.

As it is illustrated in Figure 4-14, the SNR value for 20µm radius size is higher than 15µm membrane radius size. This is due to the higher rigidity of 20µm membrane radius size of CMUT array. Furthermore, the SNR figure reveals that there is an optimum point where if the CMUT array operates at that point, Maximum value of SNR could be achieved.

According to Eq. 3-7, the collapse voltages for CMUT membrane radius of 15µm and 20µm are 180.64V and 205.77V. Figures 4-14 and 4-15 prove that if CMUT array is biased at 73% of collapse voltage, maximum SNR achieves.

CONCLUSION AND FUTURE WORK

In this thesis, an existing equivalent circuit model for analyzing the immersed CMUT array is used to find the optimal operation point of CMUT array. The CMUT array is design for operating in 20MHz. Two sets of CMUT array is designed; one which has 15µm membrane radius and another one has 20µm. For fair comparison, the gap height for both designs chose to be 100nm and analysis of arrays is done based on the assumption that biased voltage and driven AC voltage are applied such that maximum deflection will occur. Furthermore, due to the lack of an appropriate equivalent circuit model for radiation impedance, FEM simulation is done to obtain the behavior of radiation impedance for wide range of ka. It has been proved that although there is a peak value for real part of radiation impedance in specific ka product which was reported by other researchers; however there is a peak value at the same ka product for imaginary part of radiation impedance. Furthermore, radiation impedance is implemented by circuit component into the equivalent circuit model and CMUT array pulse-echo performance, receive sensitivity and SNR are studied. It has been proved

that if CMUT array biased in 73% of collapse voltage, the best signal-to-noise ratio achieves which is the key factor in ultrasonic imaging.

It is worthwhile to mention that a model for diffraction loss and attenuation in the propagation medium should be incorporated for future work. Also in this analysis it has been assumed that CMUT is working in infinite number cells and the radiation impedance is modeled according to this assumption. However we know that CMUT cell numbers are finite. Even though the model is correct for CMUT cells which located in the center of array, however those which are located at the age of array won't observe the same radiation impedance due to the impedance coupling affect. So a model for finite number of cells should be incorporate to better model the acoustic cross-talk.

Reference:

[1] H. T. Soh, I. Ladabaum, A. Atalar, C. F. Quate, and B. T. Khuri-Yakub, "Silicon micromachined ultrasonic immersion transducers," *Appl. Phys. Lett.*, vol. 69, pp. 3674–3676, 1996.

[2] I. Ladabaum, X. Jin, H. T. Soh, F. Pierre, A. Atalar, and B. T. Khuri-Yakub, "Microfabricated ultrasonic transducers: Towards robust models and immersion devices," in *Proc. IEEE Ultrason. Symp*, 1996, pp. 335–338.

[3] A. Burhdorf, O. Ahrens, and J. Binder, "Capacitive Micromachined ultrasonic transducers and their application," in *Proc. IEEE Ultrason. Symp.*, 2001, pp. 933–940.

[4] J. S. McIntosh, D. A. Hutchins, G. Etcheverry, D. R. Billson, R. A. Noble, R. R. Davies, and L. Koker, "Micromachined capacitive transducer array for imaging in air," in Proc. IEEE Ultrason. Symp, 2001, pp. 929–932.

[5] J. S. McIntosh, D. A. Hutchins, D. R. Billson, T. J. Robertson, R. A. Noble, and A. D. R. Jones, "The characterization of capacitive micromachined ultrasonic transducers in air," Ultrasonics, vol. 40, pp. 477–483, 2002.

[6] J. Johnson, ¨ O. Oralkan, U. Demirci, S. Ergun, M. Karaman, and B. T. Khuri-Yakub, "Medical imaging using capacitive Micromachined ultrasonic transducer arrays," Ultrasonics, vol. 40, pp. 471–476, 2002.

[7] O. Oralkan, A. S. Ergun, J. A. Johnson, M. Karaman, U. Demirci, K. Kaviani, T. H. Lee, and B. T. Khuri-Yakub, "Capacitive micromachined ultrasonic transducers: Next generation arrays for acoustic imaging?," in IEEE Trans. Ultrason., Ferroelect., Freq. Contr., vol. 49, pp. 1596–1610, 2002.

[8] O. Oralkan, A. S. Ergun, C.-H. Cheng, J. A. Johnson, M. Karaman, T. H. Lee, and B. T. Khuri-Yakub, "Volumetric ultrasound imaging using 2-D cMUT arrays," in IEEE Trans. Ultrason., Ferroelect., Freq. Contr., vol. 50, pp. 1581–1594, 2003.

[9] F. Yalcin Yamaner, Selim Olcum, H. Kagan Oguz, Ayhan Bozkurt, Hayrettin Koymen, Abdullah Atalar, "High-Power CMUTs: Design and Experimental Verification" in IEEE Trans. Ultrason., Ferroelect., Freq. Contr., vol. 59, pp. 1276–1284, 2012

[10] F. Yalcin Yamaner, Selim Olcum, Ayhan Bozkurt, Hayrettin Koymen, Abdullah Atalar, "Optimizing CMUT Geometry for High Power", in Proc. IEEE Ultrason. Symp., 2010, pp. 2247–2250

[11] A. Bozkurt, F. L. Degertekin, A. Atalar, and B. T. Khuri-Yakub, "Analytic modelling of loss and cross-coupling in capacitive Micromachined ultrasonic transducers," in Proc. IEEE Ultrason. Symp. 1998, pp. 1025–1028.

[12] I. Ladabaum, X. Jin, H. T. Soh, A. Atalar, and B. T. Khuri- Yakub, "Surface micromachined capacitive ultrasonic transducers," IEEE Trans. Ultrason., Ferroelect., Freq. Contr., vol. 45, pp. 678–690, 1998.

[13] A. Caronti, G. Caliano, A. Iula, and M. Pappalardo, "An accurate model for capacitive micromachined ultrasonic transducers," IEEE Trans. Ultrason., Ferroelect., Freq. Contr., vol. 49, pp. 159–167, 2002.

[14] A. Nikoozadeh, B. Bayram, G. G. Yaralioglu, and B. T. Khuri- Yakub, "Analytical calculation of collapse voltage of cMUT membrane," in Proc. IEEE Ultrason. Symp., 2004, pp. 256–259.

[15] S. Hansen, N. Irani, F. L. Degertekin, and B. T. Khuri-Yakub, "Defect imaging by Micromachined ultrasonic air transducers", in Proc. IEEE Ultrason. Symp, 1998, pp. 1003-1007.

[16] I. Ladabaum, X. Jin, H. T. Soh, A. Atalar, and B. T. Khuri- Yakub, "Surface Micromachined capacitive ultrasonic transducer" , IEEE Trans. Ultrason., Ferroelect., Freq. Contr.,, vol. 45, no. 3, pp. 678-690, 1998.

[17] G. Caliano, R. Carotenuto, E. Cianci, V. Foglietti, A. Caronti, A. Iula, and M. Pappalardo, "Design, fabrication and characterization for a capacitive micromachined

ultrasonic probe for medical imaging", IEEE Trans. Ultrason., Ferroelect., Freq. Contr., vol. 52, no. 12, pp. 2259-2269, 2005.

[18] Omer Oralkan, Sean T. Hansen, Baris Bayram, Goksen G. Yaralioglu, A. Sanli Ergun, and Butrus T. Khuri-Yakub, "High Frequency CMUT arrays for High Resolution Medical Imaging", in Proc. IEEE Ultrason. Symp, 2004, pp. 399-402.

[19] M. Legros, C. Meynier, R. Dufait, and F. Tranquart, "Piezocomposite and CMUT array asessment through in vitro imaging performance", in Proc. IEEE Ultrason. Symp, 2008, pp. 1142-1145.

[20] I. O. Wygant, X. Zhuang, D. T. Yeh, O. Oralkan, A. S. Ergun, M. Karaman, and B. T. Khuri-Yakub, "Integration of 2D CMUT array with front-end electronics for volumetric ultrasound imaging" , IEEE Trans. Ultrason., Ferroelect., Freq. Contr., vol. 55, no. 2, pp. 327-342, 2008.

[21] Jaime Zahorian, Michael Hochman, Toby Xu, Sarp Satir, Gokce Gurun, Mustafa Karaman, and F. Levent Degertekin, "Monolithic CMUT-on-CMOS Integration for Intravascular Ultrasound Application " , IEEE Transactions of Ultrasonics, Ferroelectrics and Frequency control, vol. 58, no. 12, pp. 2659-2667, 2011

[22] D. M. Mills, "Medical imaging with capacitive micromachined ultrasonic transducer (CMUT) arrays", in Proc. IEEE Ultrason. Symp, 2004, pp. 384-390.

[23] G. Caliano, R. Carotenuto, E. Cianci, V. Foglietti, A. Caronti, A. Iula, and M. Pappalardo, "Design, fabrication and characterization for a capacitive micromachined ultrasonic probe for medical imaging" , IEEE Trans. Ultrason., Ferroelect., Freq. Contr., vol. 52, no. 12, pp. 2259-2269, 2005

[24] Y. Huang, E. O. H_ggstr•om, X. Zhuang, A. S. Ergun, and B. T. Khuri-Yakub, "Optimized membrane configuration improves CMUT performance", in Proc. IEEE Ultrason. Symp, 2004, pp. 505-508.

[25] R. Guldiken, M. Balantekin, J. Zahorian, and F. Degertekin, \Characterization of dual-electrode CMUTs: demonstration of improved receive performance and pulse echo

47

operation with dynamic membrane shaping," Ultrasonics, Ferroelectrics and Frequency Control, IEEE Trans. Ultrason., Ferroelect., Freq. Contr., vol. 55, no. 10, pp. 2336-2344, 2008.

[26] R. Guldiken, J. McLean, and F. Degertekin, "CMUTs with dual electrode structure for improved transmit and receive performance", IEEE Trans. Ultrason., Ferroelect., Freq. Contr., vol. 53, no. 2, pp. 483-491, 2006.

[27] S. Machida, S. Migitaka, H. Tanaka, K. Hashiba, H. Enomoto, Y. Tadaki, and T. Kobayashi, "Analysis of the charging problem in capacitive micro-machined ultrasonic transducers" , in Proc. IEEE Ultrason. Symp, 2008, pp. 383 -385.

[28]. C. Goldsmith, J. Ehmke, A. Malczewski, B. Pillans, S. Eshelman, Z. Yao, J. Brank, and M. Eberly, "Lifetime characterization of capacitive RF MEMS switches" , in Microwave Symposium Digest, 2001 IEEE MTT-S International, 2001, pp. 227 -230 vol.1.

[29] H. Martinussen, A. Aksnes, and H. Engan, "Investigation of charge diffusion in CMUTs using optical interferometry", in Proc. IEEE Ultrason. Symp, 2008, pp. 1218 - 1221.

[30] Y. Huang, E. Haggstrom, B. Bayram, X. Zhuang, A. Ergun, C. Cheng, and B. Khuri-Yakub, "Collapsed regime operation of capacitive micromachined ultrasonic transducers based on wafer-bonding technique" , in Proc. IEEE Ultrason. Symp, 2003, pp.1161-1164

[31] Y. Huang, E. Haggstrom, B. Bayram, X. Zhuang, A. Ergun, C. Cheng, and B. Khuri-Yakub, "Collapsed regime operation of capacitive micromachined ultrasonic transducers based on wafer-bonding technique", in Proc. IEEE Ultrason. Symp, 2003, pp. 1161-1164.

[32] B. Bayram, M. Kubnik, G. G. Yaralioglu, O. Oralkan, A. S. Ergun, D.S. Lin, S. H. Wong, and B. T. Khuri-Yakub, "Finite element modeling and experimental characterization of crosstalk in 1-D CMUT arrays" IEEE Trans. Ultrason., Ferroelect., Freq. Contr., vol. 54, no. 2, pp. 418-428, 2007.
48

[33] M. Wilm, A. Reinhardt, V. Laude, R. Armati, W. Daniau, and S. Ballandras, "Three-dimensional modeling of micromachined-ultrasonic transducer arrays operating in water" , IEEE Trans. Ultrason., Ferroelect., Freq. Contr., vol. 43, no. 6, pp. 457-465, 2005.

[34] I. Ladabaum, P. Wagner, C. Zanelli, J. Mould, P. Reynolds, and G. Wojcik, "Silicon substrate ringing in microfabricated ultrasonic transducers", in Proc. IEEE Ultrason. Symp, 2000, pp. 943-946.

[35] M. Wilm, A. Reinhardt, V. Laude, R. Armati, W. Daniau, and S. Ballandras, "Three-dimensional modelling of micromachined-ultrasonictransducer arrays operating in water", IEEE Trans. Ultrason., Ferroelect., Freq. Contr., vol. 43, no. 6, pp. 457-465, 2005.

[36] I. Ladabaum and P. A. Wagner, "Microfabricated ultrasonic transducer with suppressed substrate modes", Patent, March, 2005, united States Patent, Patent no: US 6862254B2.

[37] X. Jin, Omer Oralkan, L. Degertekin, and B. T. Khuri-Yakub, "Characterization of one-dimensional capacitive micromachined ultrasonic immersion transducer arrays" , IEEE Trans. Ultrason., Ferroelect., Freq. Contr., vol. 48, no. 3, pp. 750-760, 2001

[38] Hayrettin Koymen, Abdullah Atalar, Elif Aydogdu, Coskun Kocabas, H. Kagan Oguz, Selim Olcum, Alper Ozgurluk, Asli Unlugedik, "An Improved Lumped Element Nonlinear circuit model for Circular CMUT Cell", IEEE Trans. Ultrason., Ferroelect., Freq. Contr., vol. 59, no. 8, pp. 1791-1799, 2012

[39] Muhammed N. Senlik, Selim Olcum, Hayrettin Koymen, Abdullah Atalar, "Radiation Impedance of An Array of Circular Capacitive Micromachined Ultrasonic Transducer", IEEE Trans. Ultrason., Ferroelect., Freq. Contr., vol. 57, no. 4, pp. 969-976, 2010

[40] Online: [Accessed July 20, 2014], URL: http://en.wikipedia.org/wiki/Sonar.

[41] K. K. Shung, "Diagnostic ultrasound: Past, present, and future", Journal of Medical and Biological Engineering, vol. 31, no. 6, pp. 371-374, 2011.

[42] Johan M. Thijssen, Gert Weijers, and Chris L. De Korte. "Objective performancetesting and quality assurance of medical ultrasound equipment", *Ultrasound in Med. & Biol.*, 33, No. 3, pp 460–471, 2007.

[43] B. Bayram, E. Haggstrom, G. G. Yaralioglu, and B. T. Khuri-Yakub, "A new regime for operating capacitive micromachined ultrasonic transducers",IEEE Trans. Ultrason., Ferroelect., Freq. Contr., vol. 50, no. 9, pp. 1184-1190, 2003.

[44] Y. Huang, E. Haggstrom, B. Bayram, X. Zhuang, A. Ergun, C.-H. Cheng, and B. Khuri-Yakub, "Comparison of conventional and collapsedregion operation of capacitive micromachined ultrasonic transducers", IEEE Trans. Ultrason., Ferroelect., Freq. Contr., vol. 53, no. 10, pp. 1918 -1933, 2006.

[45] I. O. Wygant, M. Kupnik, and B. T. Khuri-Yakub, "Analytically calculatingmembrane displacement and the equivalent circuit model of acircular CMUT cell,"in Proc. IEEE Ultrason. Symp, 2008,pp. 2111–2114.

[46] I. O. Wygant, M. Kupnik, and B. T. Khuri-Yakub, "CMUT Design Equations for Optimizing Noise Figure and Source Pressure", in Proc. IEEE Ultrason. Symp, 2009,

[47] Goksen G. Yaralioglu, Baris Bayram, and B. T. Khuri-Yakub, "Finite Element Analysis of CMUTs: Conventional vs Collapse Operation Mode" in Proc. IEEE Ultrason. Symp., 2006, pp. 586-589.

[48] W. Mason, *Electromechanical Transducers and Wave Filters". 2nd ed.* VanNostrand, New York, 1948.

[49] M. Greenspan, "Piston radiator: Some extensions of the theory," *AcousticalSociety of America Journal*, vol. 65, pp. 608–621, Mar. 1979.

[50] H. Kagan Oguz, Selim Olcum, Muhammed N. Senlik, Abdullah Atalar, Hayrettin Koymen, "A novel Equivalent Circuit Model for CMUT", in Proc. IEEE Ultrason. Symp., 2009, pp. 2193-2196.

50

[51] C. Meynier, Franck Teston, and Dominique Certon, "A multiscale model for array of capacitive micromachined ultrasonic transducers,"*J. Acoust. Soc. Am.,* vol. 128, pp. 2549-2561, 2010.

[52] H. Kagan Oguz, Abdullah Atalar, Hayrettin Koymen, "Equivalent Circuit-Based Analysis of CMUT cell Dynamics in Arrays", IEEE Trans. Ultrason., Ferroelect., Freq. Contr., vol. 60, no. 5, pp. 1016 -1024, 2013.

[53] Butrus T Khuri-Yakub and O¨ mer Oralkan, "Capacitive Micromachined Ultrasound Transducers for Medical Imaging and Therapy", J. micromech. And microeng., vol. 21, 2011

51